NASA TECHNICAL NOTE

NASA TN D-6606

NASA TN D-6606

DYNAMIC BEHAVIOR OF AIR LUBRICATED PIVOTED-PAD JOURNAL-BEARING — ROTOR SYSTEM

II - Pivot Consideration and Pad Mass

by Zolton N. Nemeth

Lewis Research Center
Cleveland, Ohio 44135

NATIONAL AERONAUTICS AND SPACE ADMINISTRATION • WASHINGTON, D. C. • FEBRUARY 1972

1. Report No. NASA TN D-6606	2. Government Accession No.	3. Recip.
4. Title and Subtitle DYNAMIC BEHAVIOR OF AIR LUBRICATED PIVOTED-PAD JOURNAL-BEARING - ROTOR SYSTEM II - PIVOT CONSIDERATION AND PAD MASS		5. Report Date February 1972 6. Performing Organization Code
7. Author(s) Zolton N. Nemeth		8. Performing Organization Report No. E-6336
9. Performing Organization Name and Address Lewis Research Center National Aeronautics and Space Administration Cleveland, Ohio 44135		10. Work Unit No. 114-03 11. Contract or Grant No.
12. Sponsoring Agency Name and Address National Aeronautics and Space Administration Washington, D.C. 20546		13. Type of Report and Period Covered Technical Note 14. Sponsoring Agency Code
15. Supplementary Notes		

16. Abstract

Rotor bearing dynamic tests were conducted with tilting-pad journal bearings having three different pad masses and two different pivot geometries. The rotor was vertically mounted and supported by two three-pad tilting-pad gas journal bearings and a simple externally pressurized thrust bearing. The bearing pads were 5.1 cm (2.02 in.) in diameter and 3.8 cm (1.5 in.) long. The length to diameter ratio was 0.75. One pad was mounted on a flexible diaphragm. The bearing supply pressure ranged from 0 to 690 kilonewtons per square meter (0 to 100 psig), and speeds ranged to 38 500 rpm. Heavy mass pad tilting-pad assemblies produced three rotor-bearing resonances above the first two rotor critical speeds. Lower supply pressure eliminated the resonances. The resonances were oriented primarily in the direction normal to the diaphragm.

17. Key Words (Suggested by Author(s))
Bearing
Gas bearing
Pivoted-pad journal bearing

18. Distribution Statement
Unclassified - unlimited

19. Security Classif. (of this report)	20. Security Classif. (of this page)	21. No. of Pages	22. Price*
Unclassified	Unclassified	42	$3.00

* For sale by the National Technical Information Service, Springfield, Virginia 22151

DYNAMIC BEHAVIOR OF AIR LUBRICATED PIVOTED-PAD JOURNAL-BEARING - ROTOR SYSTEM II - PIVOT CONSIDERATION AND PAD MASS

by Zolton N. Nemeth

Lewis Research Center

SUMMARY

Experiments were conducted with three masses of tilting-pad journal bearings and three rotors. The bearings were operated both pressurized and self-acting. Two types of pivot geometries were used: conforming and nonconforming. The vertical rotor was supported by the two three-pad tilting-pad, air-lubricated, journal bearings and a simple externally pressurized thrust bearing. The bearing pads were 5.1 centimeters (2.02 in.) in diameter and 3.8 centimeters (1.5 in.) long. The length to diameter ratio was 0.75. Each pad was individually pivoted. Two of the pivots were rigidly mounted, and the third was soft flexure mounted. The diaphragm flexure stiffness was approximately 7.6×10^5 newtons per meter (4300 lbf/in.). The bearings were preloaded at zero speed to 53 newtons (12 lbf). Tests were run over a speed range of 0 to 38 500 rpm.

Heavy mass pads produced three rotor bearing resonances above the rotor first and second critical speeds. Shaft motions at resonance were usually oriented perpendicular to the face of the diaphragm flexure. The second resonance was a combination of motions perpendicular and parallel to the face of the diaphragm flexure. The amplitude of these resonant motions and the speed range through which large amplitudes persist increase with pad mass. These motions may be eliminated by decreasing the lubricant supply pressure. Rotor axial resonance was produced above the second rotor bearing resonance from 20 000 to 23 500 rpm with heavy mass tilting-pad journal bearings.

Pivot surface damage was minimal for the two geometry pivots under most conditions. High-impact pivot surface damage was sustained by the rigidly mounted nonconforming pivots when operated at high supply pressure at the first rotor critical speed.

INTRODUCTION

Tilting-pad gas journal bearings, rather than other simpler types of gas journal bearings, are used to support the rotating assembly in the Brayton (gas) cycle space turbomachinery (refs. 1 to 5) and other high-speed machines because they are more stable and reliable (ref. 5). The simpler gas bearing, like the plain circular bearing, exhibit fractional frequency whirl instability under light loading within the operating speed range of high speed machines. In most applications, a tilting-pad bearing can be designed so that fractional frequency whirl is either nonexistent or has a threshold speed well above the operating speed (ref. 6). The tilting-pad journal bearing can compensate for centrifugal growth and thermal expansion in high-speed and high-temperature machines.

The complex tilting-pad journal bearing with its multiplicity of parts could introduce additional motions and problems. Some of these motions and problems were identified in the experimental work with three-pad tilting-pad gas journal bearings reported in part I of this investigation (ref. 7). Reference 7 showed negligible pad resonances and no fractional frequency whirl. The speed range was from 0 to 38 500 rpm with pressurized and self-acting modes. Reference 7 reported on the effect of flexure (diaphragm) pivot-support stiffness and damping on pad and rotor-bearing system performance.

The present study is a continuation of this earlier investigation (ref. 7). The objectives of the present investigation were to (1) determine the effect of pad mass, pivot geometry, and air supply pressure on pad and rotor-bearing system dynamics, (2) explore the effect of rotor construction (thermal heat shunt) on bearing operation and (3) observe the effects of the above on the operation of the self alining gimbal supported pressurized thrust bearing.

The bearing selected for testing was similar to the bearings used in the Brayton rotating unit (BRU) (ref. 2). The bearings used in this investigation were 5.1 centimeters (2.02 in.) in diameter and 3.8 centimeters (1.50 in.) long. The bearings in the Brayton machinery were 4.4 centimeters (1.75 in.) in diameter and 3.3 centimeters (1.31 in.) long. The bearing length-to-diameter ratio L/D was 0.75 in each case. The diaphragm stiffness was 7.6×10^5 newtons per meter (4300 lbf/in.). Diaphragm stiffnesses of 3.5×10^5 to 7.0×10^5 newtons per meter (2000 to 4000 lbf/in.) were used in the Brayton cycle turbocompressor (ref. 8). The clamping force was 53 newtons (12 lbf) as in reference 7.

The test tilting-pad journal bearings were operated to 38 500 rpm under pressurized and self-acting modes. The thrust bearing is only capable of operation under pressurization. Air was used as the lubricant.

SYMBOLS

C radial clearance, μm; in.

D bearing (rotor) diameter, cm; in.

d orifice diameter, μm; in.

K diaphragm stiffness, N/m; lbf/in.

L bearing length, cm; in.

N shaft speed, rpm

R bearing radius, cm; in.

APPARATUS

Bearing Test Apparatus

A schematic view and photograph of the pivoted-pad gas journal bearing test apparatus are shown in figure 1. The bearing apparatus consisted of a vertically oriented rotor supported by two identical tilting-pad journal bearings and a thrust bearing at the lower end of the rotor. The rotor had an air turbine mounted on the upper end, two journal sections 28 centimeters (11 in.) apart, and a thrust surface at the lower end. The vertically oriented rotor is used to simulate a gravity-free load environment on the journal bearings.

Each journal bearing assembly (pivot mount and pad) is mounted on an individual support. The supports may be adjusted radially to position the bearing assembly as required and to preload the bearing initially at zero pressurization to obtain the desired clamping load.

Bearings

Tilting-pad bearing. - A schematic view of the air-lubricated, tilting-pad journal bearing with instrumentation is shown in figure 2. The bearing pads are self-acting (hydrodynamic) with provisions for pressurized operation. The bearing consists of three curved pads. Each pad is individually pivoted. Two of the pads are supported on rigid mounts. The third pad is supported on a low-spring-rate flexure to accommodate radial growth of the rotor and to lower the critical speed and bearing loads at the critical speeds. With a low-spring-rate flexure, the pads have to be loaded against the rotor at

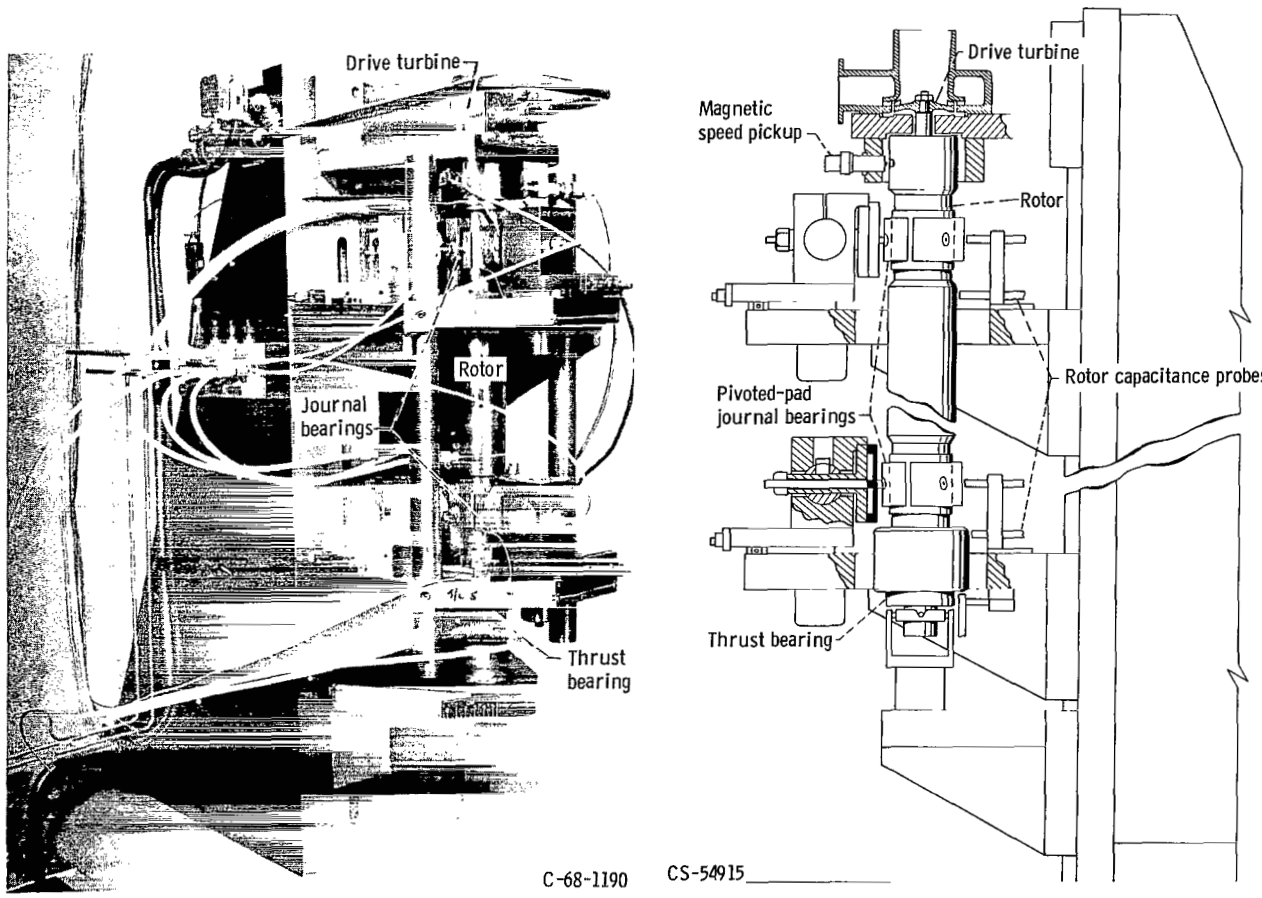

Figure 1. - Pivoted-pad gas journal bearing test apparatus.

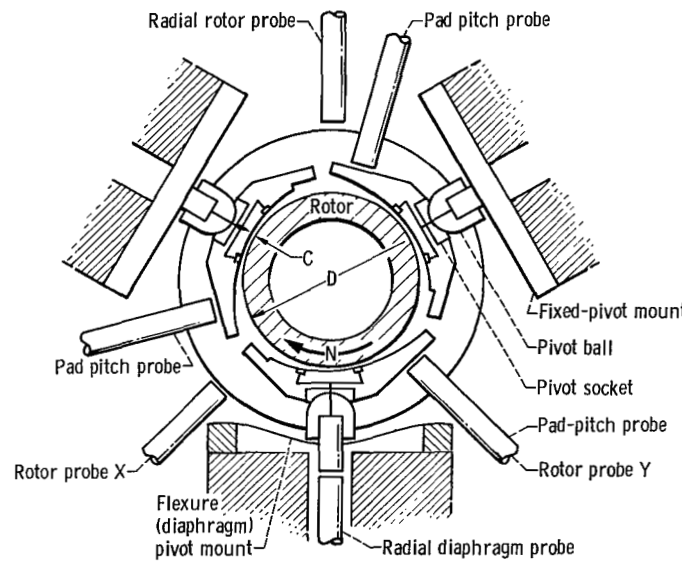

Figure 2. - Tilting-pad journal bearing with instrumentation.

zero speed (this load is called clamping load) to maintain preload (a condition where the pivot clearance is less than the machined-in clearance) at design speed. This is necessary for stable operation of the pads in pitch, roll, and yaw. The use of clamping load requires pressurized operation at startup and to an intermediate speed (approximately 20 000 rpm for the present setup) where self-acting operation becomes possible.

Bearing pads. - A view of two of the three pads of different masses investigated is shown in figure 3. The heavy mass pad is not shown; it looks much like the medium

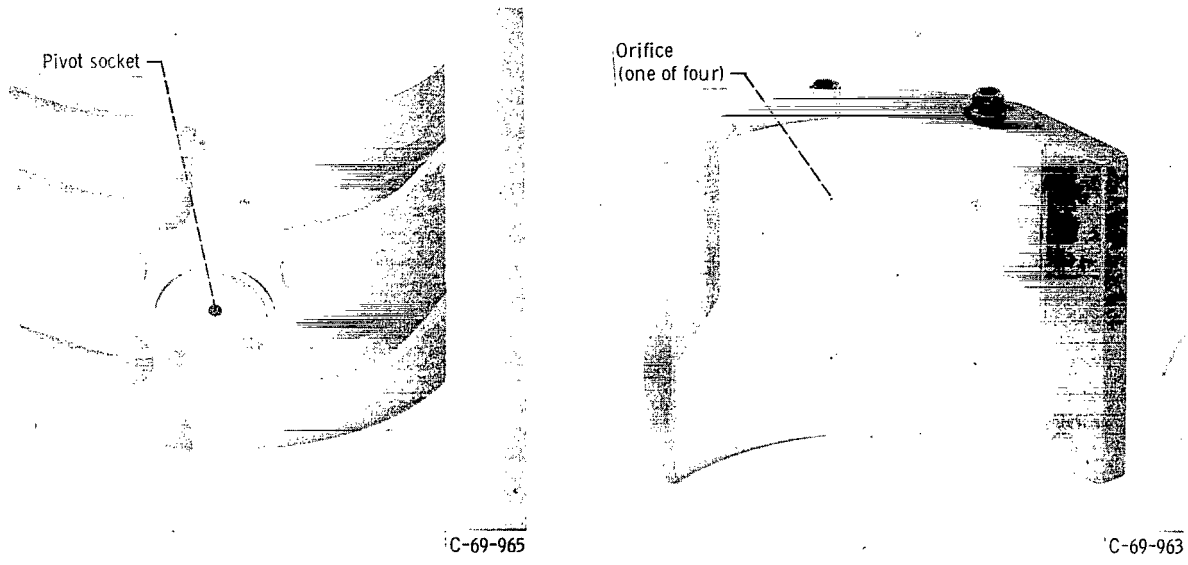

(a) Light mass pad.

(b) Medium mass pad.

Figure 3. - Bearing pads.

mass pad. Each bearing assembly contained three identical pads of the same mass. Each pad had an active arc length of 100^{o}. The weight of the pad with pivot socket and mass moments of inertia in the pitch and roll modes are given in table I. The moments of inertia of the pads were measured by pendulation. The medium mass pad was reported on in reference 7. Two additional pad weights were investigated in the present study: one lighter and one heavier than the pads reported in reference 7.

The pads had pivots that were located 65^{o} from the pad leading edge. The heavier pads had four 250-micrometer (0.010-in.) diameter orifices per pad. The low mass pads each had one 500-micrometer (0.020-in.) diameter orifice.

The pads were 3.8 centimeters (1.5 in.) long and had an internal diameter of 5.1 centimeters (2.02 in.). The L/D ratio was 0.75. The machined-in radial clearance between the pad and rotor was 45.7 micrometers (0.0018 in.) for the medium mass pads and 60 micrometers (0.0023 in.) for the low and heavy mass pads.

TABLE I. - BEARING PAD CHARACTERISTICS

Pad and pivot combination[a]		Weight of pad and pivot socket		Weight of pad, pivot socket, and ball		Radial machined-in clearance		Mass moment of inertia of pad (with pivot socket)			
Number	Description	N	lbf	N	lbf	μm	in.	Pitch		Roll	
								$kg\text{-}m^2$	$lb\text{-}in.\text{-}sec^2$	$kg\text{-}m^2$	$lb\text{-}in.\text{-}sec^2$
1	Low mass pad, conforming pivot	0.445	0.100	0.534	0.120	60	0.0023	1.19×10^{-5}	0.105×10^{-3}	1.06×10^{-5}	0.0934×10^{-3}
2	Medium mass pad, conforming pivot	1.00	0.225	(b)	(b)	45.7	0.0018	3.50×10^{-5}	0.310×10^{-3}	2.81×10^{-5}	0.249×10^{-3}
3	Heavy mass pad, conforming pivot	1.14	0.256	1.23	0.276	60	0.0023	3.94×10^{-5}	0.349×10^{-3}	3.45×10^{-5}	0.305×10^{-3}
4	Heavy mass pad, nonconforming pivot	1.39	0.312	1.55	0.348	60	0.0023	7.99×10^{-5}	0.707×10^{-3}	7.37×10^{-5}	0.652×10^{-3}

[a]Pivot location from pad leading edge for all pads is 65°.

[b]Not applicable. Pivot ball is part of diaphragm.

Pivots. - A schematic view of each of the pivot geometries investigated is shown in figure 4. Basically, there were two pivot geometries: a conforming and a nonconforming ball and socket. There were two conforming pivot types. Conforming I was integral with the pad and diaphragm flexure. Conforming II was replaceable in the bearing pad and diaphragm flexure.

Pressurized gas is fed through the pivot to the pad surface at startup and at the lower speeds. Gas sealing is obtained in the conforming geometry by lapped ball-socket sur-

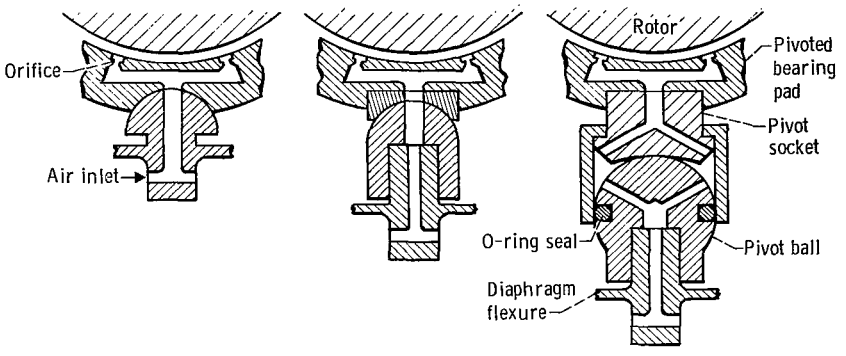

(a) Conforming I. (b) Conforming II. (c) Nonconforming.

Figure 4. - Pivoted-pad bearing pivots and jacking gas system.

faces. The feed hole is through the center of the pivot assembly. Gas sealing is obtained in the nonconforming pivot by an O-ring seal. The feed holes are located in the area between the O-ring seal and the ball-socket contact zone. The air supply passages are shown in figure 4.

The conforming ball and socket pivot had a radius of 0.64 centimeter (0.25 in.); the nonconforming pivot had a ball radius of 0.79 centimeter (0.31 in.) and a socket radius of 2.1 centimeters (0.81 in.). The weight of the pad with pivot socket and pivot ball is given in table I.

Diaphragm. - The diaphragm design was fully described in reference 7. Briefly, the flexible diaphragm consisted of a thin circular steel plate. The stiffness of the diaphragm could be varied by controlling its thickness. The stiffness used in these tests was 7.6×10^5 newtons per meter (4300 lbf/in.) for each tilting-pad journal bearing. Initially, before pressurizing the journal bearing, each diaphragm was set up to give a clamping load of 53 newtons (12 lbf). The diaphragms were not provided with damping in these tests.

Thrust bearing. - A view of the externally pressurized thrust bearing is shown in figure 5. It has no self-acting capability. The bearing can support the rotor at zero rotation.

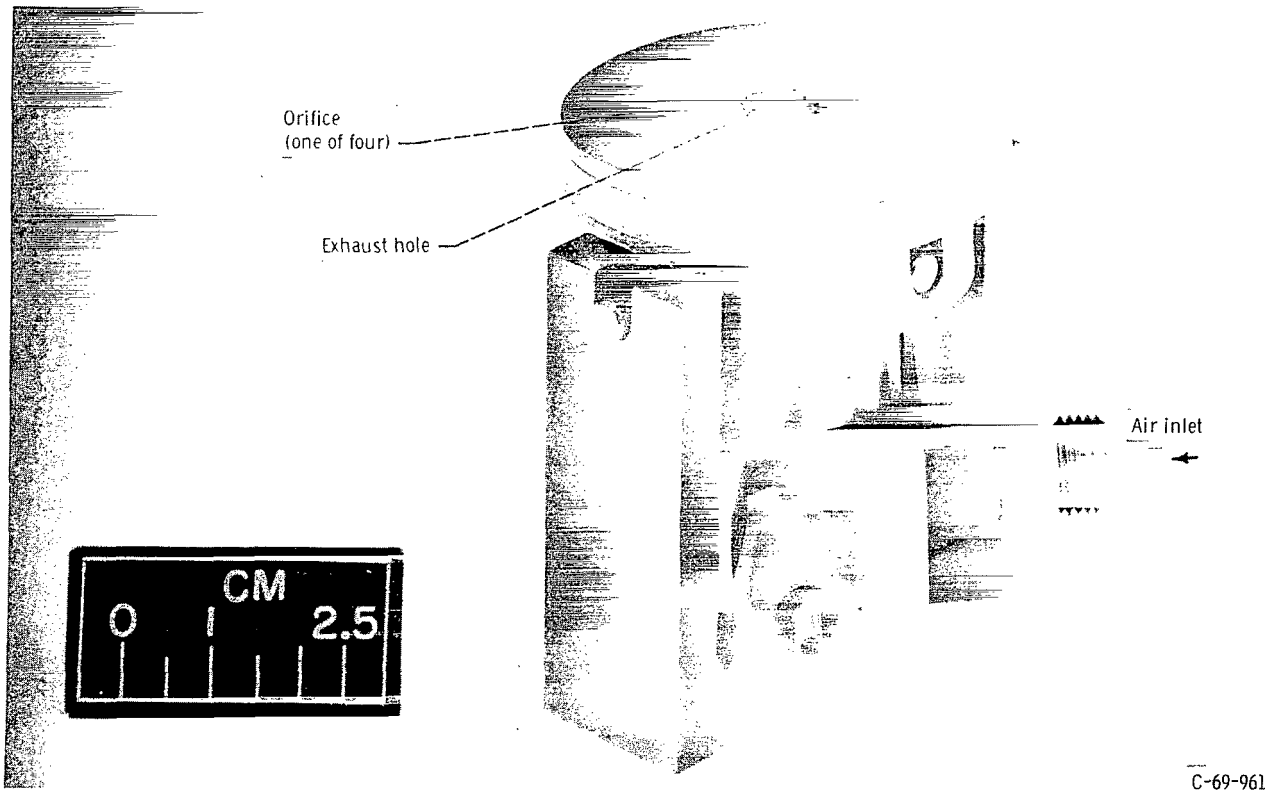

Figure 5. - Externally pressurized thrust bearing with self-alining gimbal support.

The stator plate has four 250-micrometer (10-mil) diameter orifices. It is mounted on a gimbal support to provide alinement and tracking with the rotor thrust surface at the lower end of the rotor. The stator was 5.1 centimeters (2.0 in.) in diameter and had a central exhaust hole 1.0 centimeter (0.40 in.) in diameter.

Rotor

The test rotor is shown in figure 6. The rotor was hollow with a 0.64-centimeter (0.25-in.) wall at journal locations. Three rotors were used in the investigation designated as a, b, and c. Rotor a (of ref. 7) had a thermal heat shunt; rotors b and c did not. The thermal heat shunt consisted of a heavy silver plate on the shaft inner surface at the journal locations. The rotors had mass and inertial properties nominally similar to those of the rotor in the Brayton cycle turbocompressor (ref. 1). The overall length of the rotor was 50.8 centimeters (20.0 in.), and the bearing span was 28 centimeters (11.0 in.). The rotors were not axially symmetric. The center of gravity was 12.2

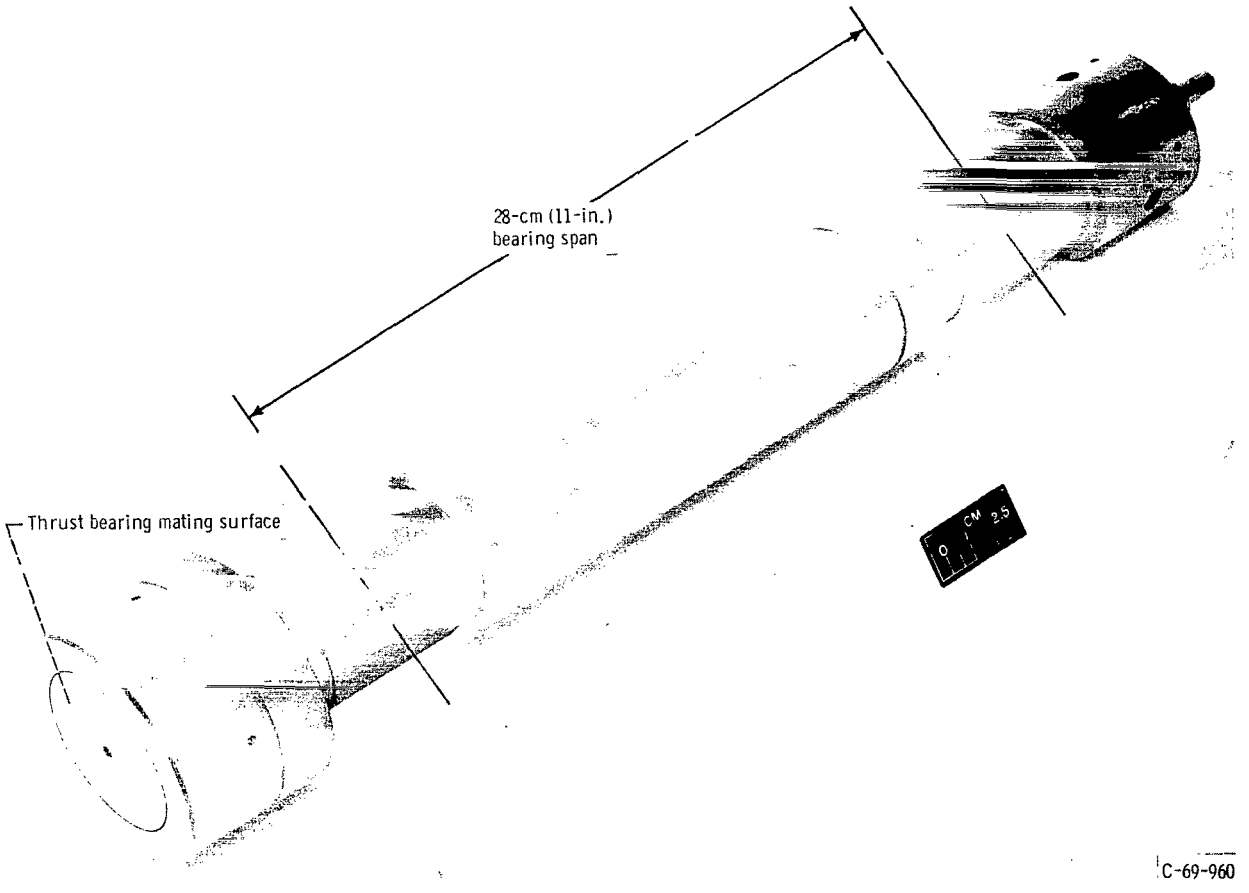

Figure 6. - Test rotor.

centimeters (4.8 in.) above the centerline of the lower journal. The rotors were of a double overhung design. The turbine and compressor wheel masses and location were simulated by mass concentrations at the ends of the rotor. The measured weight of the rotor with heat shunts was 7.4 kilograms (16.5 lbm) and of the rotors without the heat shunts was 6.7 kilograms (14.7 lbm).

The rotor was balanced as a rigid body in a commercial balancing machine at low speed (about 1800 rpm) and then checked in place in the test rig in test bearings at somewhat higher speeds (12 000 to 15 000 rpm). Check of balance in place indicated that no final correction was necessary and the center of gravity eccentricity was approximately 2.5 micrometers (0.0001 in.).

Lubrication and Air Supply System

Service air was used for pressurized operation of the test journal, the thrust bearing, and the turbine drive. The air was conditioned to remove moisture, oil vapor, and solid particles. The pressure was individually regulated to each bearing.

Ambient air in the room was used for self-acting operation of the test journal bearings. The temperature was kept at a constant 297 K (75° F).

Instrumentation

Capacitance probes. - The displacements and vibrations of the rotor, the bearing pad, and flexure (diaphragm) pivot mount were measured by capacitance probes. The capacitance probe location is shown in figures 1 and 2. There are seven probes at each journal bearing, and there is one probe at the end of the rotor to observe its axial motion. Two more probes were used in some tests to observe the effect of speed on the bending of the shaft. Movements as small as 0.25 micrometer (10 μin.) could be discerned. The accuracy of the readout instrument was approximately ±3 percent.

The purposes of the probes were as follows: At each journal bearing two probes, designated X and Y, were used to observe the rotor center motion. The X and Y probes were located symmetrically about the axis of the flexure diaphragm. A third probe observed flexure diaphragm radial motion. A fourth probe was used to monitor the motion of rotor in line with the axis of the flexure diaphragm and was placed 180° from the flexure diaphragm probe. Three probes were used to observe the pitch motion of each of the three pads. These probes were located on the centerline of each pad and directed toward the center of the bearing.

Tape system and readout. - A 14-channel FM tape recorder was used to record the speed of rotation, time of day, and 12 capacitance-vibration signals. All of the recording was made at 38 centimeters per second (15 in./sec) for recorder response flat from dc to 5 kilohertz.

The readout instruments were oscilloscopes, peak-to-peak amplitude meter, phase meter, X-Y recorder, and an optical recording potentiometer. Readout could be obtained at any time after the experiment from the permanent record on the tape recorder.

Speed measurement and control. - Rotor speed was measured by a magnetic probe and indicated on an electronic counter. Six shallow holes on the upper diameter of rotor produced a signal in the magnetic probe that gave a count directly in rpm on the counter.

PROCEDURE

Pad mass and pivot tests were conducted simultaneously under the pressurized then the self-acting mode. The intention was to test the various pivot geometries with each pad mass in succession. However, not all pivots were operated with each pad mass because of pad damage under certain operating conditions. One bearing, the lower journal tilting-pad bearing (with three pads) was considered to be the test bearing; the same as in part I of this investigation (ref. 7). The upper bearing rotor response was similar to the lower bearing rotor response but not exactly like it because the rotor was not symmetrical. The two journal tilting-pad bearings, the upper and lower, were identical in geometry and pivot configuration. Identical stiffness diaphragms were used for both the upper and lower journal bearings in this investigation.

The data were obtained during coastdown from a maximum speed of 38 500 rpm. Coastdown took approximately 8 minutes under pressurized operation of the journal bearings and provided a smooth continuous speed change sufficiently slow to allow motions of rotor bearing system to develop an equilibrium maximum value at the critical speeds. With increasing speed, the speed change could not be made that slowly, and the motions did not have time to develop. Most of the tests were conducted in the externally pressurized mode over the entire coastdown speed range. Some coastdown tests were conducted in the self-acting mode to approximately 20 000 rpm and then in the externally pressurized mode to 2000 rpm. This procedure was repeated for the various pressures, pads, and pivots.

The data were continuously recorded on the tape recorder and simultaneously displayed on the oscilloscopes. Detailed observations of the data were made by replaying the tape after the test. Photographic data were obtained from the tape recorder after test. The rotor center orbit (determined by the X and Y components of motion) and the X and Y components of shaft motion against time base were obtained simultaneously with two cameras and oscilloscopes. The photographs are presented side by side in the figures of this report. Photographs were taken at maximum amplitudes of motion or at other desired times as determined by monitoring the retracing of the amplitude against rotor speed curve on an X-Y recorder.

RESULTS AND DISCUSSION

The results of the experimental investigation are presented in figures 7 to 28. The response of the rotor and bearing pads of a three-pad tilting-pad journal bearing with one pad flexure mounted is discussed for pressurized and self-acting operation over the speed range. The effects of supply pressure, pad mass, and pivot configuration are presented.

Pressurized Operation

Effect of pad mass. - The response of the rotor-bearing system with two different pad masses to rotor unbalance is shown in figure 7. The pads had conforming pivots and were operated at a supply pressure of 410 kilonewtons per square meter (60 psig). A typical response of the rotor bearing system was obtained for the medium mass pads with rotor a. Over the speed range investigated, two critical speeds were encountered with large amplitudes of rotor motion at points A and B at approximately 7500 and 11 500 rpm, respectively. Above the critical speeds, the rotor amplitude remained low and approximately constant. The maximum speed reached was about 38 500 rpm.

The response of the rotor bearing system for the low mass pads with conforming pivots is not shown because it is similar to the response of the medium mass pad rotor system. For the low mass pads, two critical speeds are also encountered with no additional resonances at the higher speeds.

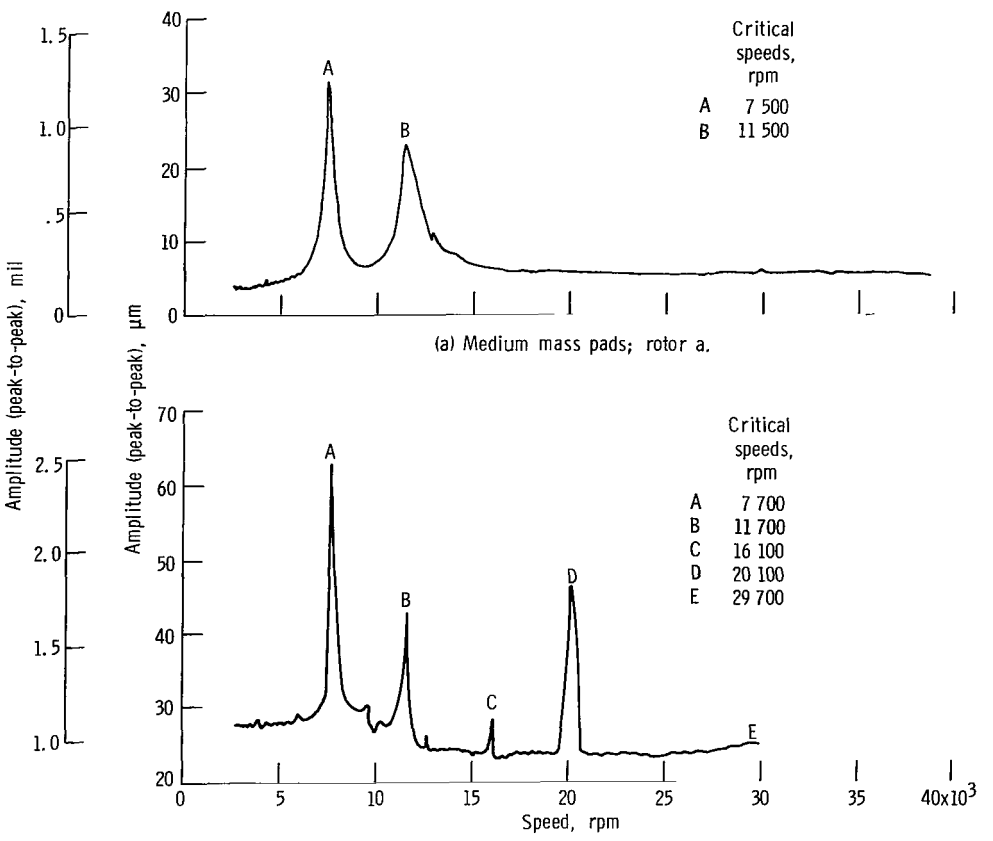

Figure 7. - Rotor response to residual unbalance with two different pad masses with conforming pivots as detected by rotor probe X. Pressurized operation at 410 kilonewtons per square meter (60 psig).

The response of the rotor bearing system with heavy mass pads over the speed range is shown in figure 7(b). In addition to the first two critical speeds at points A and B that were seen before, three other new critical speeds or resonances are encountered at higher speeds at points C, D, and E. The first two critical speeds A and B occurred at approximately 7700 and 11 700 rpm, respectively. These speeds are about the same as those for the medium mass pad critical speeds. The higher critical speeds at points C, D, and E are approximately 16 100, 20 100, and 29 700 rpm, respectively.

The three critical speeds above the first two rotor critical speeds seem to bear a speed relation with the first rotor critical speed. The first rotor critical occurs at about 7700 rpm. The critical speeds at C, D, and E occur at about 16 100, 20 100, and 29 700 rpm, respectively. These are approximately two, two and one-half, and four times the first critical speed of 7700 rpm. The reason the higher critical speeds were compared with the first critical speed will be shown later.

Another difference among the data for the medium pads and the other two mass pads (low and heavy) was thought to be more serious and limited the maximum speed of operation to 30 000 rpm. At this speed the rotor orbit became too large for safe operation. The rotor orbit size started growing with speed from about 15 000 rpm. At the time of experiment no explanation was at hand for the orbit growth. Later, additional experiments determined the cause of the orbit growth to be rotor bending. This is discussed in a later section.

The photographs in figure 8 show the rotor orbit and corresponding time-base oscilloscope traces at the critical speeds for the heavy mass pad conforming pivot combination given in figure 7(b). The large shaft markers seen in the photographs caused the background amplitude in figure 7 to be high. This did not interfere with the determination of speed, character, and size of the orbits and amplitudes in the photographs. Points A and B (figs. 8(a) and (b)) are the first and second rotor critical speeds. The rotor center motion is highly elliptical at both critical speeds because of the nonuniform stiffness around the bearing caused by two rigid pivot mounts and one soft pivot mount on a flexure diaphragm. The rotor orbit orientation is perpendicular to the diaphragm flexure at the first critical speed and parallel to it at the second critical speed. The orbits at the first two critical speeds were synchronous with the shaft rotation as can be seen from the photographs at points A and B. The photographs show a shaft marker occurring once per revolution on the time base photographs and twice on the orbit photographs (twice on the orbit since two probes are used to develop the orbit; each probe sees the shaft marker once per revolution of the rotor).

The growth of orbit size with speed is illustrated in the photograph at about 30 000 rpm at point E.

The three higher critical speeds or resonances had the following characteristics: (1) they were always oriented perpendicular to the flexure diaphragm, and (2) they were

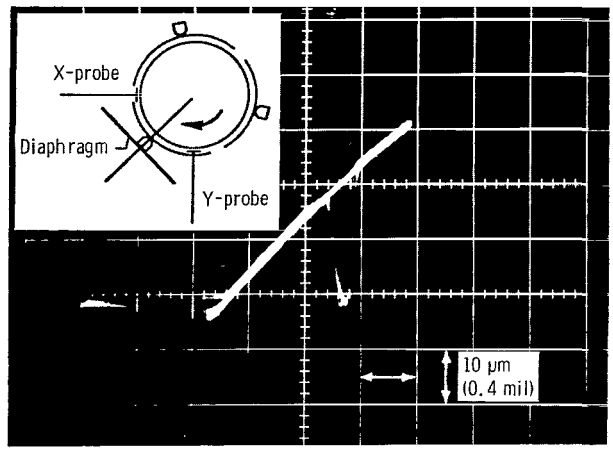

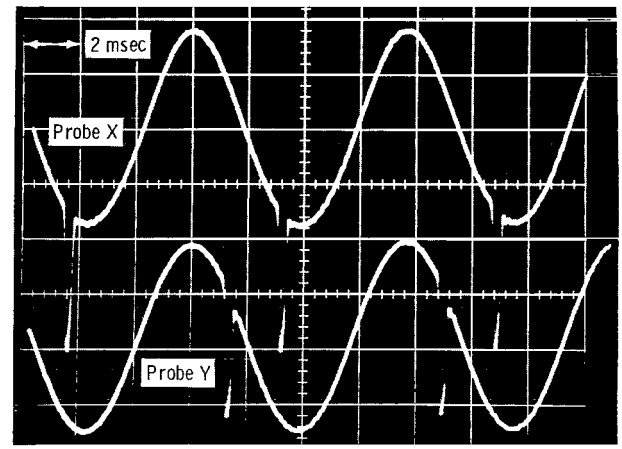

(a) Critical speed A.

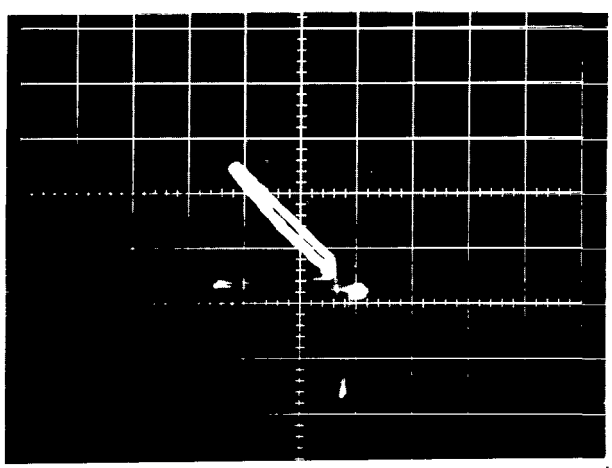

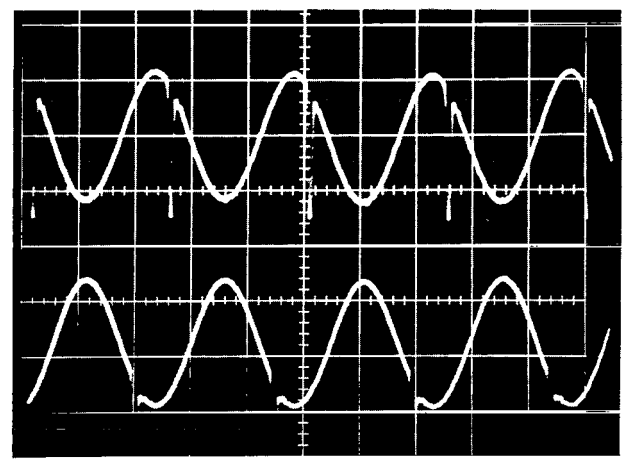

(b) Critical speed B.

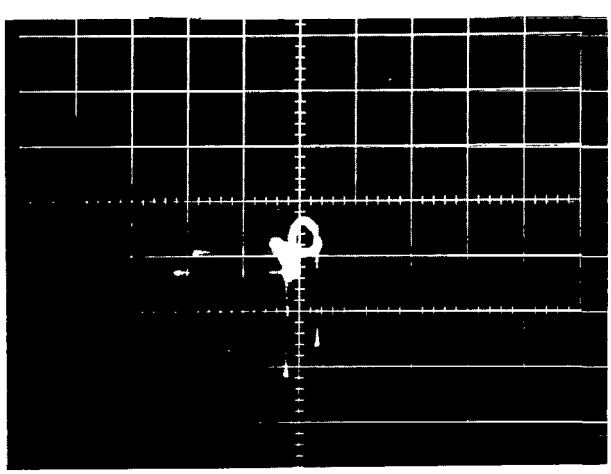

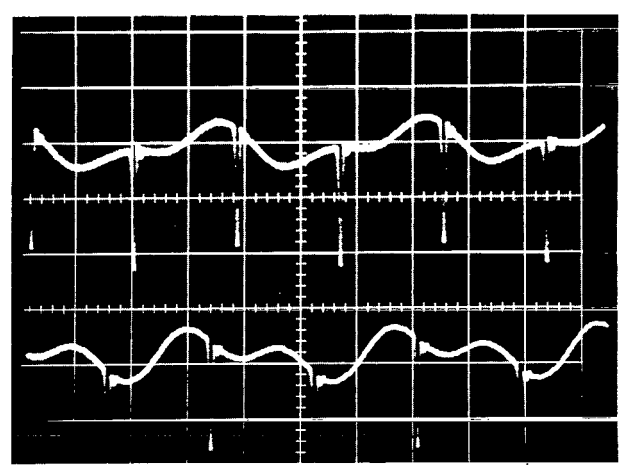

(c) Critical speed C.

Figure 8. - Oscillographs of rotor motion at various critical-speeds in figure 7(b).

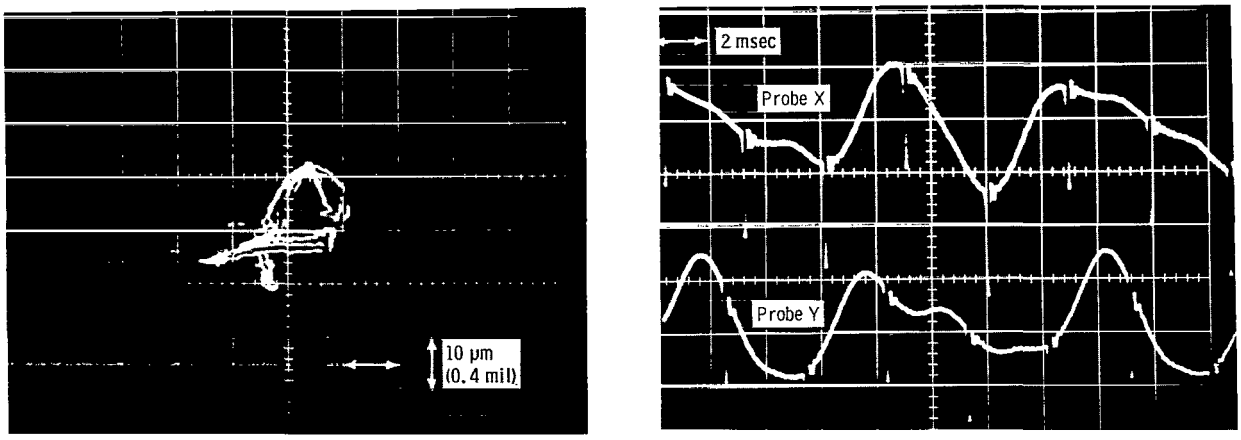

(d) Critical speed D.

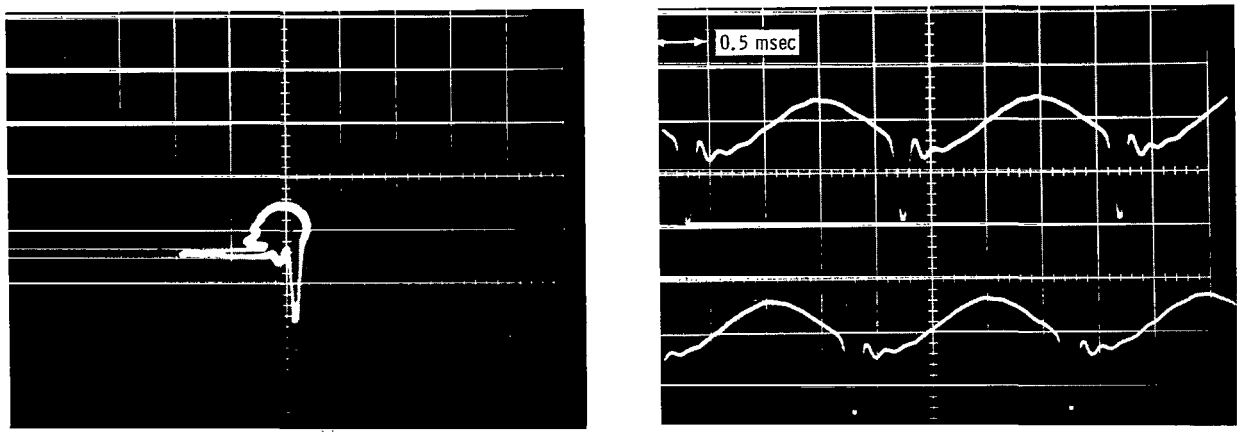

(e) Critical speed E.

Figure 8. - Concluded.

nonsynchronous. The resonance at point C (fig. 8(c)) at about 16 100 rpm rotor speed, had a frequency of about 7700 cycles per minute, which is about one-half the frequency of rotor rotation. Two sets of shaft markers are seen on the orbit photograph and on the time base photograph per cycle of resonance, which indicate that the shaft completes two revolutions for each cycle of resonance.

The resonance at point D (fig. 8(d)) at about 20 100 rpm was somewhat more complicated than the resonance at point C and seem to be a combination of motions perpendicular and parallel to the flexure diaphragm. One cycle of this combined motion took five complete revolutions of shaft to complete. The line of symmetry of motion is perpendicular to the flexure diaphragm. It can be seen from the time base curve at point D that the frequency of resonance perpendicular to the flexure diaphragm is 1/2.5 that of shaft

rotation or 8040 rpm (20 100/2.5). The frequencies of motion at points C and D are very close to the first critical speed. This and the orientation of resonance toward (perpendicular to) the flexure seems to indicate that the higher resonances are flexure resonances.

The resonance at point E at 29 700 rpm rotor speed is very slight (fig. 7(b)). The period of resonance is one-fourth the shaft speed or about 7400 cycles per minute. This again is close to first critical speed.

Effect of pivot geometry. - Figure 9 shows the response of rotor b with heavy mass pads equipped with nonconforming O-ring pivots during deceleration. The response dur-

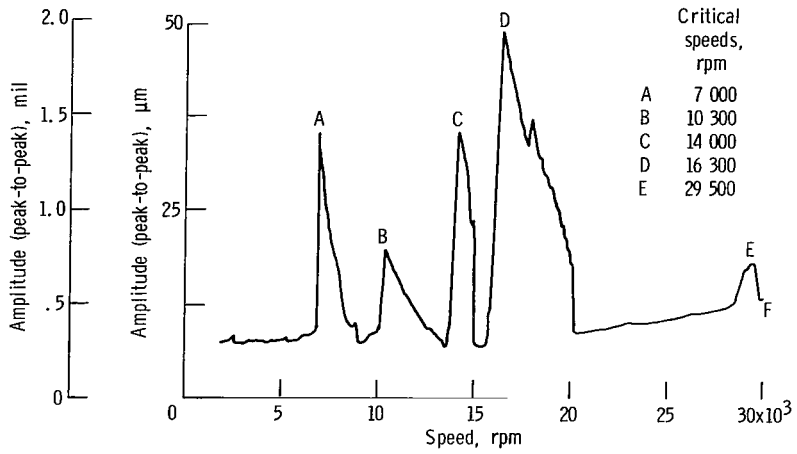

Figure 9. - Rotor b response during deceleration to residual unbalance at 410-kilonewton-per-square-meter (60-psig) supply pressure with heavy mass pads and nonconforming (O-ring) pivot as detected by rotor probe X.

ing acceleration for the same setup is shown in figure 10. It can be seen that, during acceleration, motions do not have time to develop because speed changes could not be made smoothly. The supply pressure was 410 kilonewtons per square meter (60 psig) the same as for the conforming pivot equipped heavy mass pads so that comparison can be made. It should be pointed out that the nonconforming pivot is different from the conforming pivot not only in contact geometry but also in increased weight. The total weights of the pad and pivot assembly for the two geometry pivots are 1.23 newtons (0.276 lbf) for the conforming pivot and pad and 1.55 newtons (0.348 lbf) for the nonconforming O-ring pivot and pad (table I).

The effect of the nonconforming pivot was to bring in strongly the upper three resonances at points C, D, and E (see figs. 7(b) and 9). The amplitudes and speed range over which the resonances persist were increased. This effect might be the result of in-

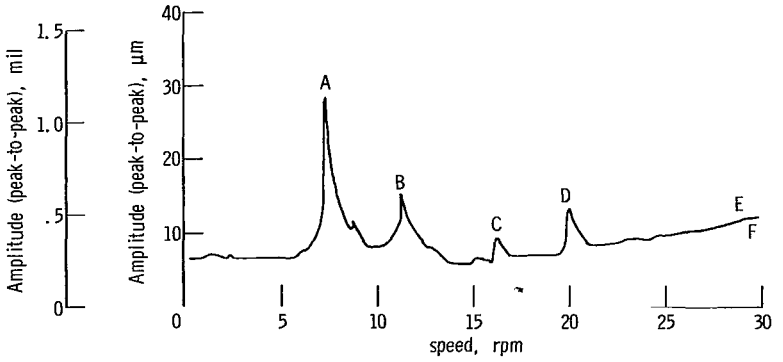

Figure 10. - Rotor response to residual unbalance during acceleration at 410-kilonewton-per-square-meter (60 psig) supply pressure with heavy mass pads and nonconforming (O-ring) pivot as detected by rotor probe X.

creased pad assembly (pad and pivot) weight as well as from the reduction in friction and damping in the pivot.

Again the rotor orbit size started to grow with increasing speed starting at about 15 000 rpm. The rotor speed was limited to a maximum of 30 000 rpm because of the large orbit size.

The three critical speeds above the first two rotor critical speeds also bear a speed relation with the first rotor critical speed. The first rotor critical occurs at about 7000 rpm. The critical speeds at C, D, and E occur at about 14 000, 16 300, and 29 500 rpm, respectively. These are approximately twice, two and one-half, and four times the first critical speed of 7000 rpm.

The resonance at E at about 29 500 rpm did not occur with increasing speed and was observed only during coastdown. Probably, the excitation force for this resonance was too small (as seen by the small amplitude), and the motion could be damped out during acceleration by existing damping forces in the bearing.

Photographs in figure 11 show the rotor motion for the heavy mass pads at various points in figure 9. The orbits at the first two critical speeds, points A and B were again elliptical and synchronous. The first critical speed was oriented perpendicular to the flexure diaphragm, and the second parallel to the flexure diaphragm. The first critical speed occurred at about 7000 rpm.

The three higher critical speeds or resonances were oriented perpendicular to the flexure diaphragm and were nonsynchronous. The resonance at point C at about 14 000 rpm rotor speed had a frequency of 7000 cycles per minute, which is one-half the frequency of rotor rotation. Two sets of shaft markers are seen on the orbit photograph and on the time base photograph per cycle of resonance. These markers indicate that the shaft completes two revolutions for each cycle of resonance.

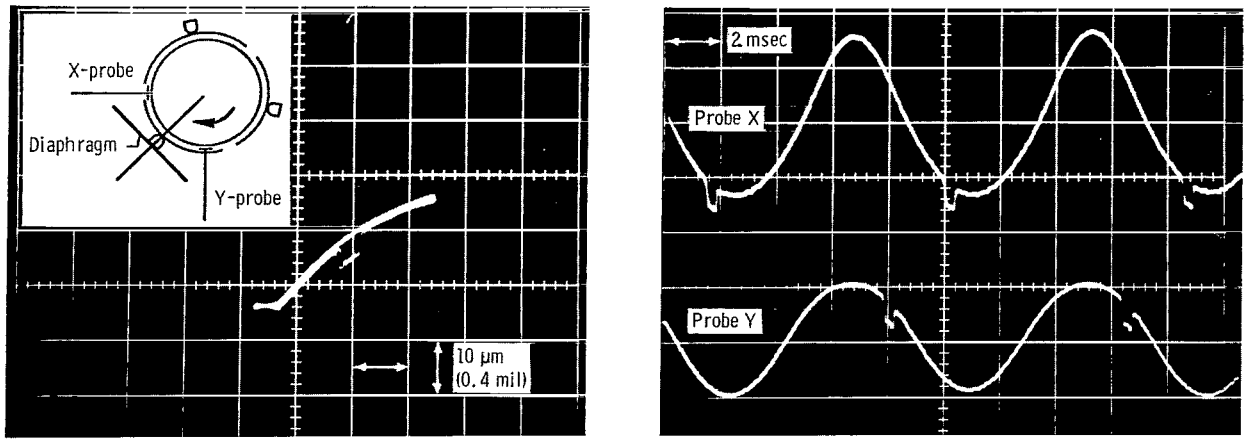

(a) Critical speed A.

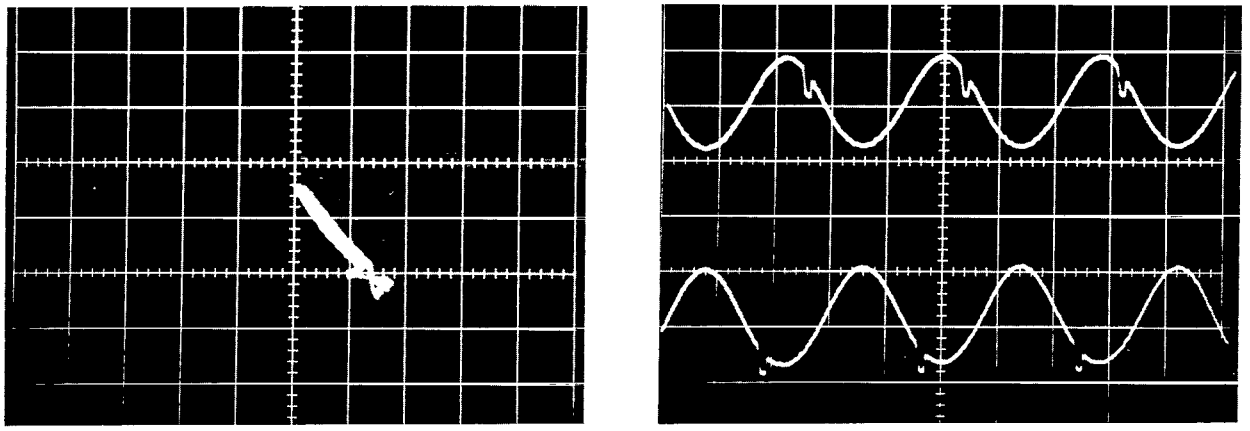

(b) Critical speed B.

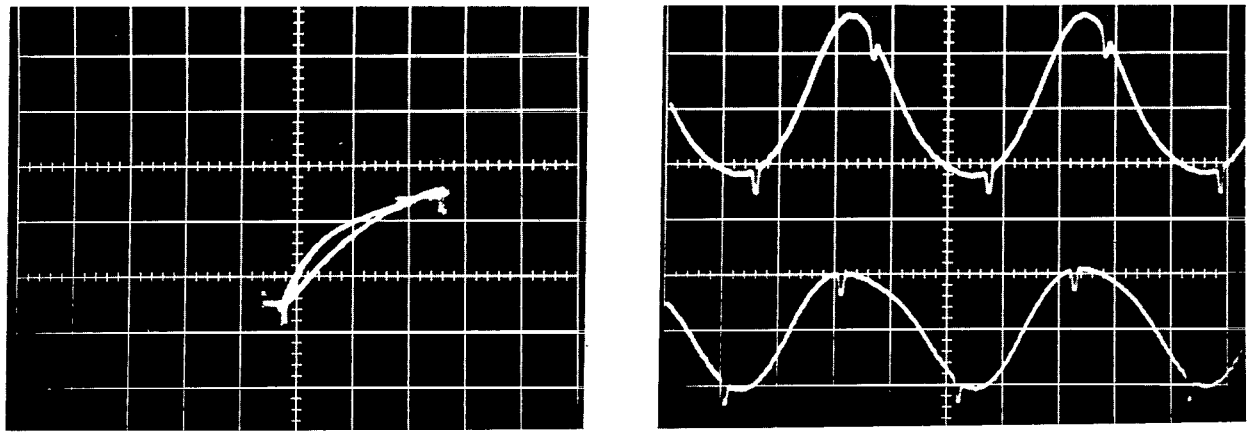

(c) Critical speed C.

Figure 11. - Oscillographs of rotor motion at various points in figure 9.

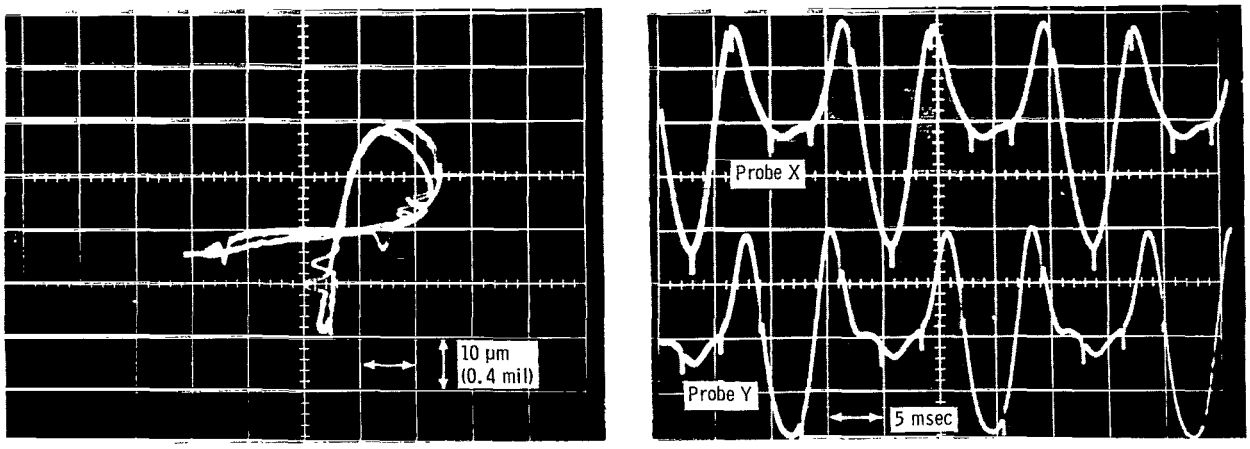

(d) Critical speed D.

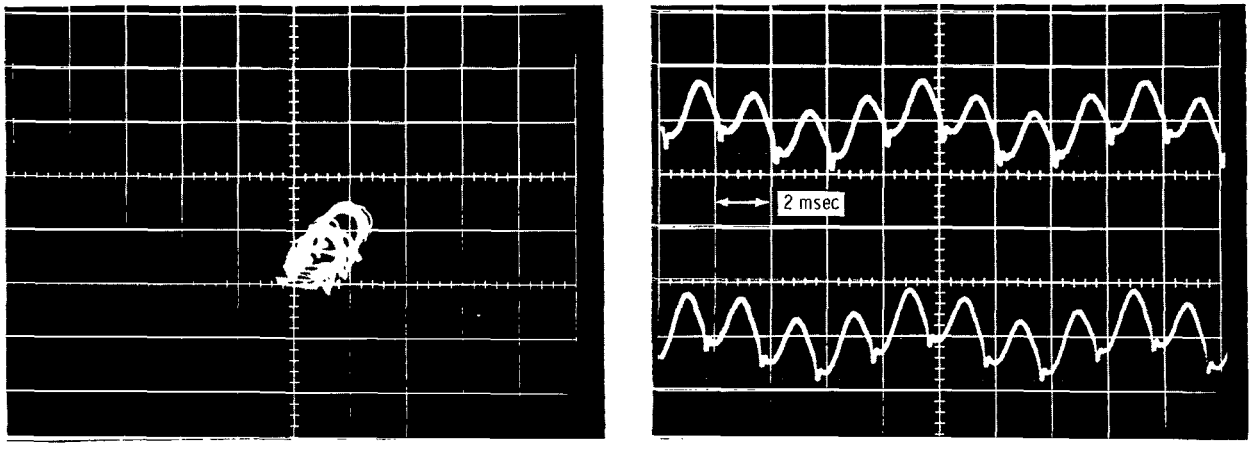

(e) Critical speed E.

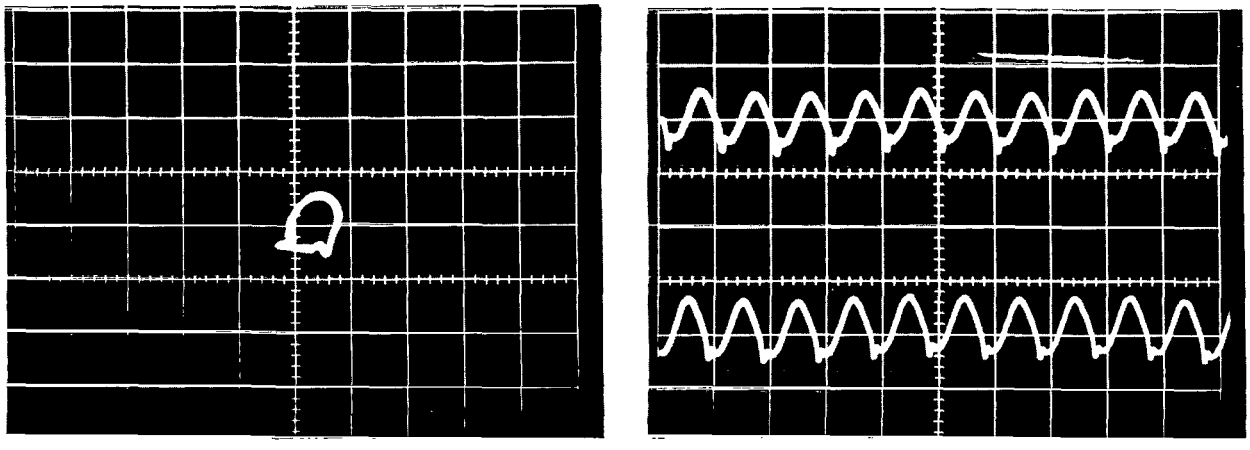

(f) Point F.

Figure 11. - Concluded.

The resonance at point D at about 16 300 rpm was a combination of motions perpendicular and parallel to the flexure diaphragm. One cycle of this combined motion took five complete revolutions of shaft to complete. The predominant motion, however, was perpendicular to the flexure diaphragm. Considering this predominant motion only, it can be seen from the time base curve at point D that its frequency of resonance is 1/2.5 that of shaft rotation or 6500 rpm (16 300/2.5). The frequencies of motion at points C and D are very close to the first critical speed.

The resonance at point E at about 29 500 rpm rotor speed is directed also perpendicular to the flexure. The period of resonance as is shown by the time base photograph is one-fourth the shaft speed or about 7370 cycles per minute. This again is close to the first critical speed.

The development of the rotor motions at points C and D in figure 9 is shown in more detail in figure 12 and in the photographs in figures 13 and 14. The motion for point C starts to develop at point C-3 (fig. 13(a)) as speed decreases (data taken during coastdown). The orbit photograph indicates an opening like an inverted V. The time-base photograph begins to show motion which is at one-half the frequency of shaft rotation. The orbit and time base photographs at point C-2 (fig. 13(b)) show the increase of this trend. At point C-1 (fig. 13(c)) the orbit has opened to a figure "8"; the time-base data clearly show the one-half frequency characteristic. The orbit and time-base data have almost reached the final motion, which is shown in photograph C. The motion at C-1 quickly snaps into the final motion and grows in amplitude from point C-1 to point C where it rapidly collapses as coastdown proceeds.

The motion at point D starts its development at point D-3 (fig. 14(a)) where the peak-to-peak amplitude abruptly increased. The motion shown by the orbit is a scramble of

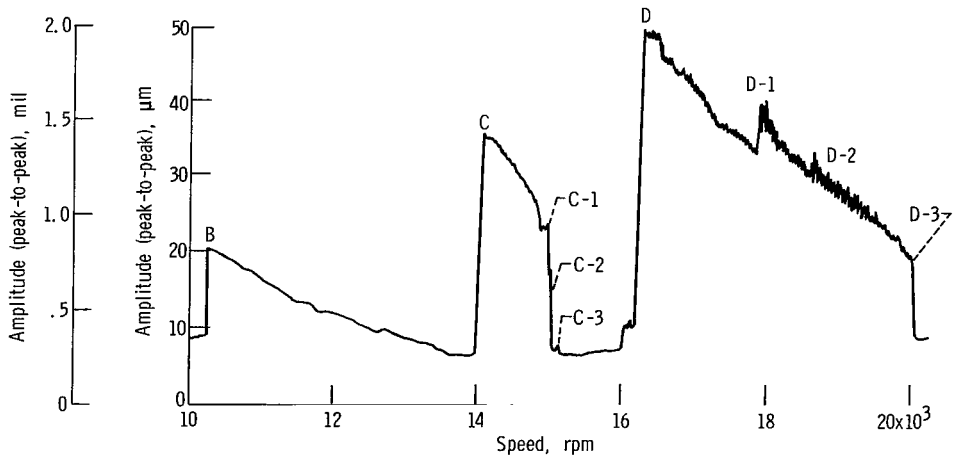

Figure 12. - Enlarged portion of figure 9 showing greater detail. Rotor response during coast down to residual unbalance at 410-kilonewton-per-square meter (60-psig) supply pressure with heavy mass pads and nonconforming (O-ring) pivot as detected by rotor probe X.

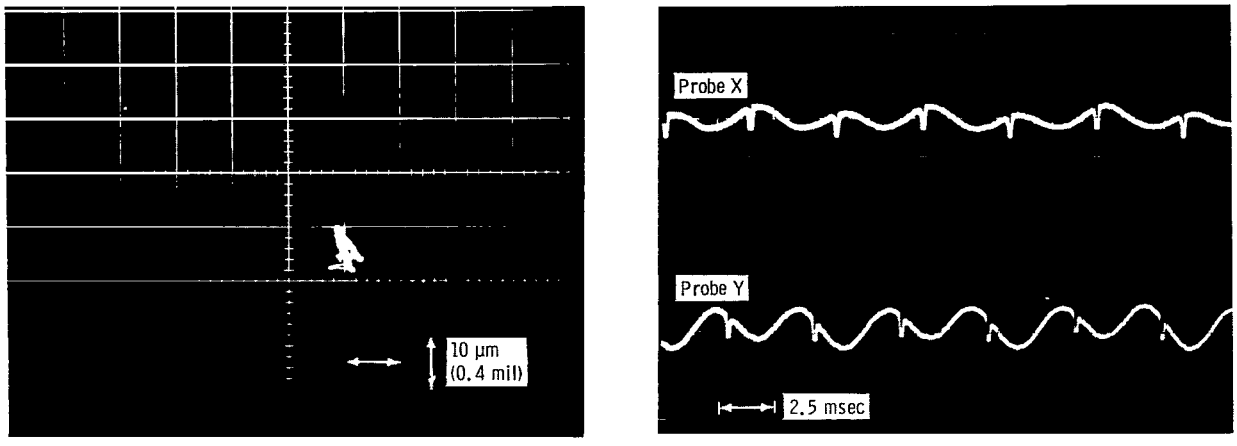

(a) Point C-3.

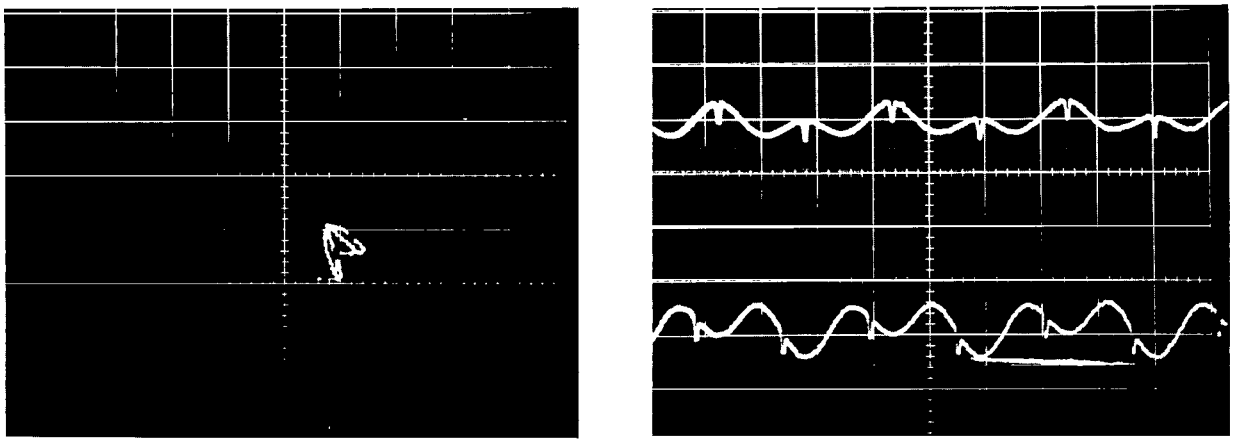

(b) Point C-2.

Figure 13. - Oscillographs of rotor motion at points C to C-3 in figure 12 showing the development of motion at point C.

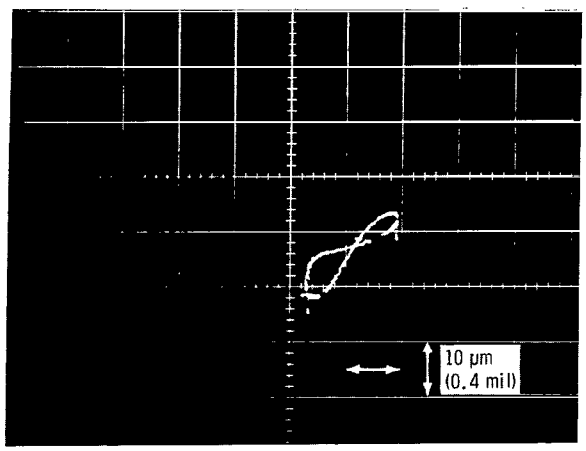

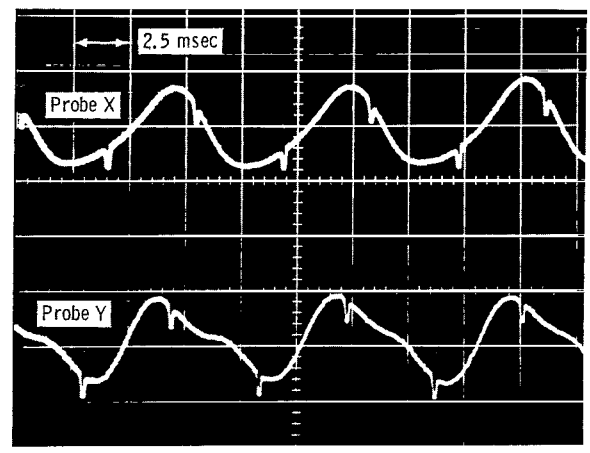

(c) Point C-1.

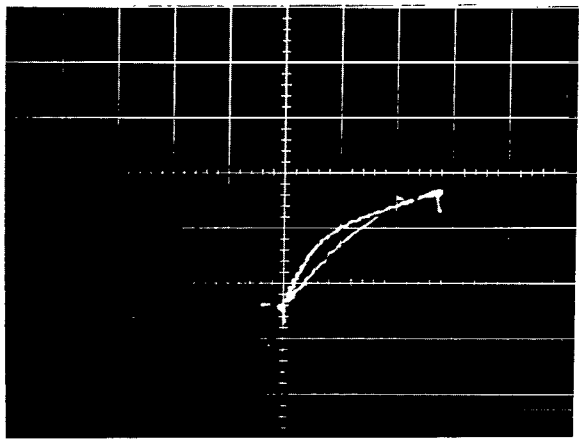

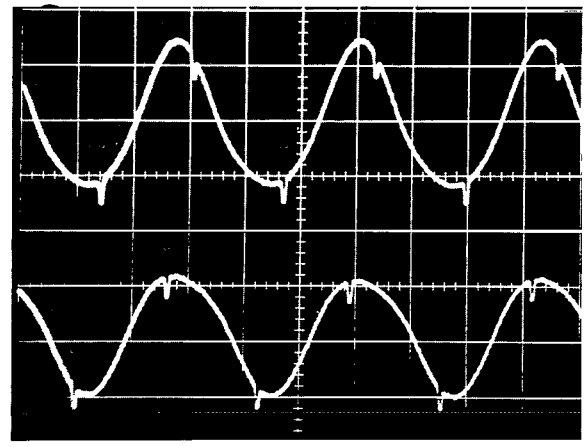

(d) Point C.

Figure 13. - Concluded.

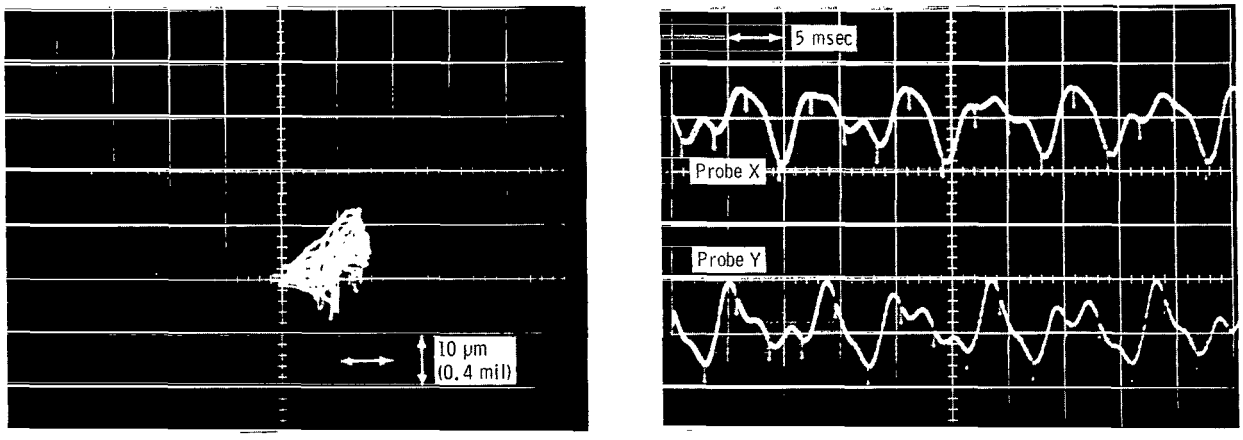

(a) Point D-3.

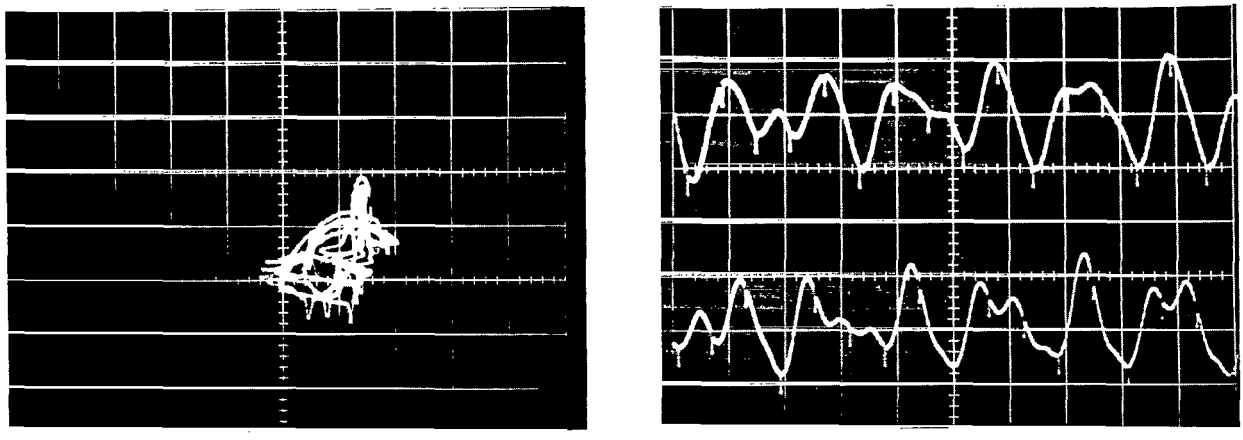

(b) Point D-2.

Figure 14. - Oscillographs of rotor motions at points D to D-3 in figure 12 showing the development of motion at point D.

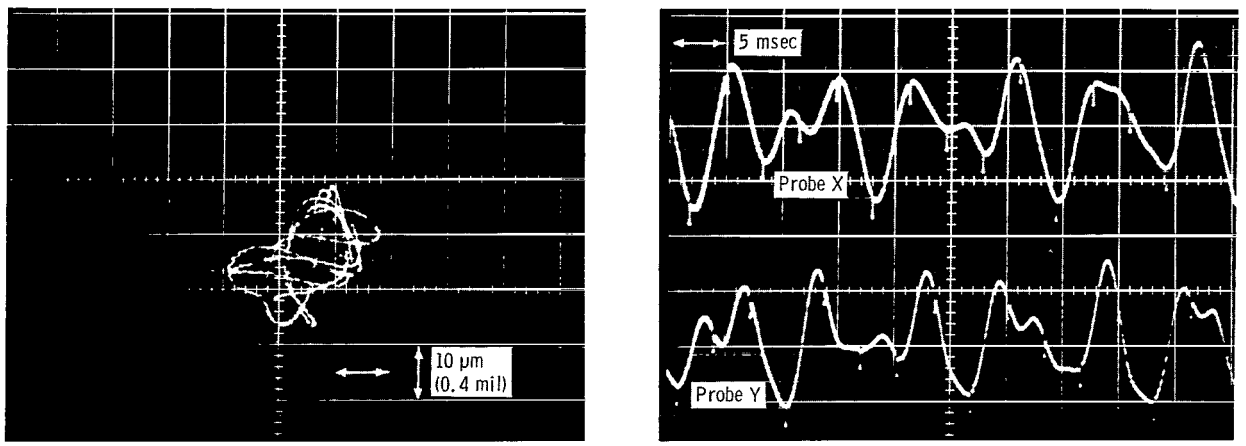

(c) Point D-1.

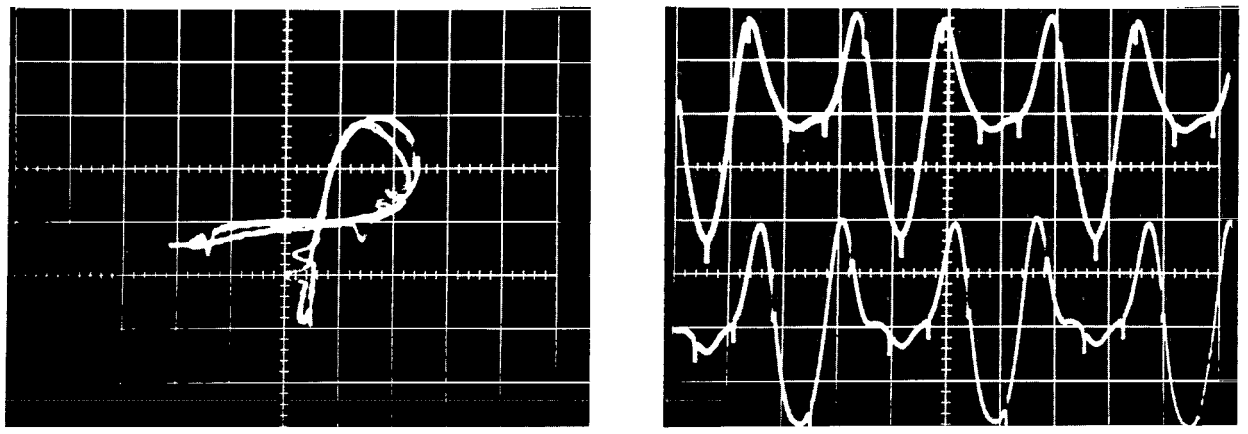

(d) Point D.

Figure 14. - Concluded.

lines, however, the time base photograph indicates the beginning of the development of a main cycle which takes five shaft revolutions to complete. As shaft speed decreases, the peak-to-peak amplitude increases and the motion develops. At point D-1 (fig. 14(c)) the motion is recognizably similar to the final motion. From a speed just below that at point D-1, the motion again quickly snaps into the final motion and grows in amplitude until the speed reaches point D (fig. 14(d)) where it rapidly collapses.

Effect of supply pressure. - The effect of increased supply pressure above 410 kilonewtons per square meter (60 psig) for the low and medium mass pads with conforming pivots was to increase the amplitude of rotor motion at the first two rotor critical speeds. No other rotor critical speeds appeared at higher speeds (ref. 7). The heavy mass pad bearings were not run at higher supply pressures because of the bad rotor-bearing response at 410 kilonewtons per square meter (60 psig) pressure and because of a pivot problem with the nonconforming pivot.

Figure 15 shows the effect of reduced supply pressure of 280 kilonewtons per square meter (40 psig) on the radial response of the rotor motion over the speed range with

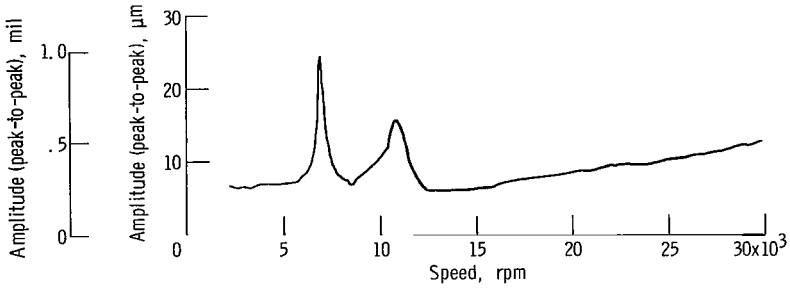

Figure 15. - Rotor response to residual unbalance at supply pressure of 280 kilonewtons per square meter (40 psig) with heavy mass pads and noncomforming (O-ring) pivot as detected by rotor probe X.

heavy mass pads and nonconforming pivots. The three higher critical speeds or resonances which appeared at the higher supply pressure (fig. 9) have disappeared entirely. The amplitude of motion at the first two critical speeds decreased from what it was at the higher supply pressure of 410 kilonewtons per square meter (60 psig). This is expected and was reported in part I (ref. 7) for the medium mass pads.

The reduction of the amplitude of motion at the first two rotor critical speed points and the elimination of the higher speed resonances at lower supply pressure were probably due to increased film damping. As supply pressure is reduced, the film thickness becomes smaller, and film damping increases (ref. 9).

A similar effect of elimination of higher resonances with reduced supply pressure was obtained for the heavy mass pads with conforming pivots.

The nonconforming O-ring pivot separated (between the pivot ball and socket) at about 550 kilonewtons per square meter (80 psig); the conforming pivot did not separate over the pressure range of the test. This is shown by the zero-speed rotor displacement curves in figure 16. The separation pressure depends on the size of the nonconforming O-ring pivot, diaphragm stiffness, and the clamping preload. Separation occurs when the pivot air-pressure force equals the pad radial load. To prevent pivot separation, the supply was limited to a maximum of 410 kilonewtons per square meter (60 psig) during most of the testing.

Operation near the pivot separation pressure leads to large impact loading and possible damage to the pivots at the rotor critical speeds (judging from the intense sound emitted). This type of preliminary operation was attempted only during balance check of the rotor.

The pivots used in this investigation were made of M-50 heat-treated steel; the same material as the tilting pads. The pivot surfaces were not coated or lubricated with any solid lubricants. No attempt was made to extend the life of the pivot contact surfaces.

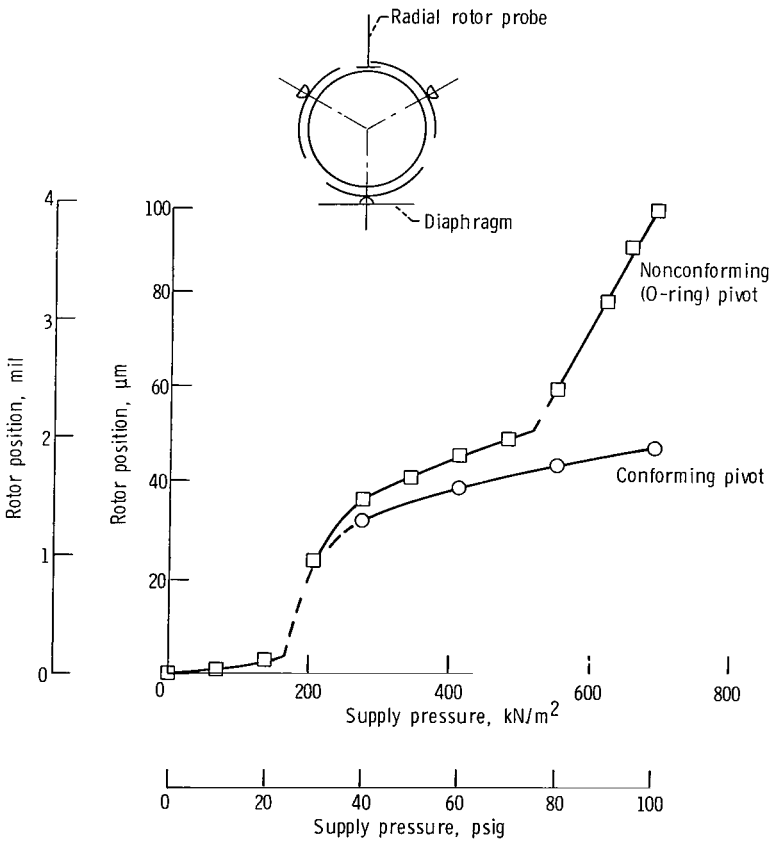

Figure 16. - Rotor position with supply pressure for two-pivot geometry.

Rather, it was desired to determine the extent of pivot damage and the cause of such damage, if possible.

The conforming pivot-socket surface before and after test with the heavy pad is shown in figure 17. Damage to surface is slight and resembles a stain because of the few hours run. The pivot-ball surface is not shown because the damage was the same and was the mirror image of the damage on the pivot socket. Surface damage occurred in the region where there is surface slippage between surfaces in an arc equidistant from the center of the pivot. Both the fixed-mounted and the flexure-mounted pivots showed about

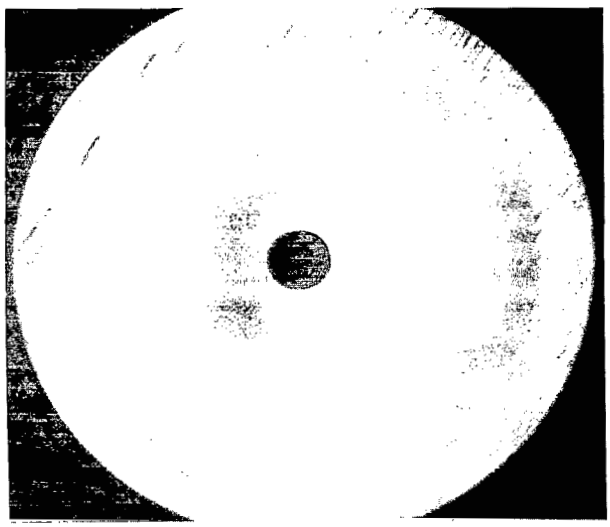

(a) New.

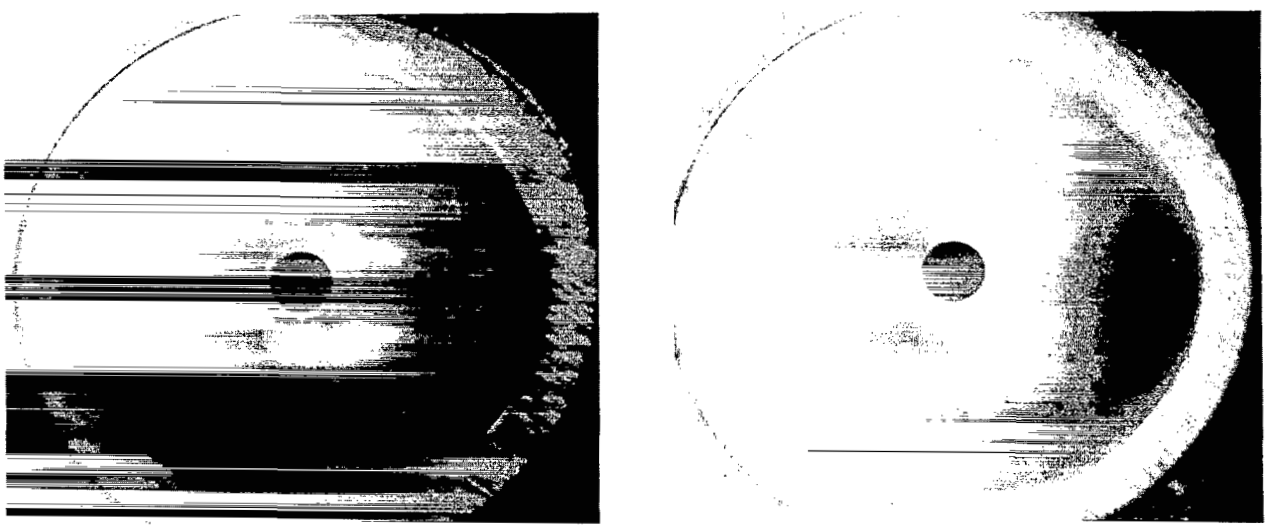

Fixed mount

Flexure (diaphragm) mount

2 mm
0.1 in.

(b) After test.

Figure 17. - Conforming pivot socket before and after test with heavy pad.

the same degree of damage. The air supply hole can be seen in the center of the pivot in the photograph in figure 17.

The nonconforming O-ring pivot had a much smaller contacting area than the conforming pivot. In spite of this, no significant surface damage was experienced during testing when the supply pressure was kept below the pivot separation pressure.

Pivot surface damage was experienced with the nonconforming O-ring pivot when the supply pressure was near the pivot separation pressure. The damage to the pivot ball and socket is shown in the photographs of figure 18. Surface damage occurred at the contact point on both fixed-mounted pivots but did not occur on the flexure mounted pivot.

Pivot damage can be detrimental to tilting-pad bearing operation even though none was experienced during this investigation. The preload can change significantly if enough material is removed from the pivot contacting surfaces.

Bearing pad response. - No pad pitch instability or resonances were observed in the course of this investigation with any of the different mass pads. Chu (ref. 10) found that the characteristic equation method predicts that a critical pitch inertia does not exist, that is, that the pad is always stable with respect to a slight disturbance from equilibrium regardless of the pitch inertia of the shoe. Also, their nonlinear orbit analysis confirmed this conclusion.

Roll motions of the pads were not available because no instrumentation was provided to observe this mode of pad motion. The roll motion mode might be the more dangerous mode, however. No evidence of difficulty due to roll motion was apparent in the course of the investigation.

Response of the diaphragm flexure pivoted pad assembly is shown in figure 19 along with the motion of the rotor for the heavy mass pad and conforming pivot at a supply pressure of 410 kilonewtons per square meter (60 psig). The rotor and pad radial capacitance probes are in the same plane but are 180° apart. The radial response of the diaphragm flexure pivoted pad was one of mainly tracking the motion of the rotor at the critical speeds at points A, B, C, and D in figure 19 and the shaft bend at point E. The phase relation of 180° evident in the photographs at points A, C, and D is simply the measure of separation of the two capacitance probes. The inphase relation of the signals at point E at 30 000 rpm is because of and is the measure of shaft bend. The rotor and diaphragm probes were on the opposite sides of the nodal point.

Phase measurements by electronic instrumentation at speed regions other than the large motion producing regions of the critical speed points and resonances was not feasible. The small motions produced unsteady small voltages that could not be indicated by the phase instrumentation.

Axial rotor response. - With light mass pads, no rotor-axial response was evident with speed (see fig. 20(a)). With medium mass pads, there was no axial response of the rotor except for a small amplitude resonance of about 10 micrometers (0.4 mil) at ap-

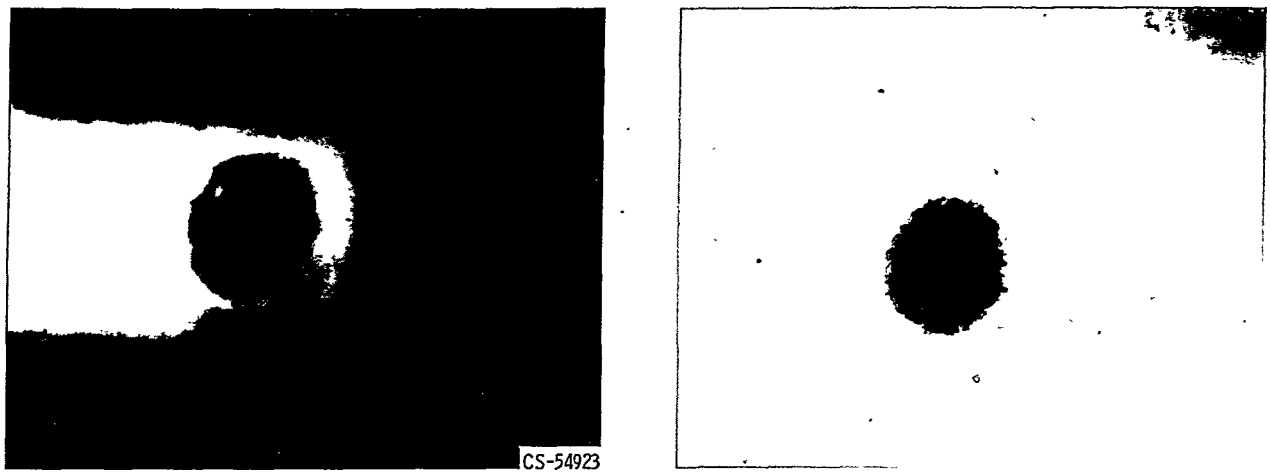

(a) Fixed mounted 1.

(b) Fixed mounted 2.

(c) Flexure (diaphragm) mounted.

0.05 mm
(0.02 in.)

Figure 18. - Nonconforming O-ring pivot after test with heavy pad in the lower bearing.

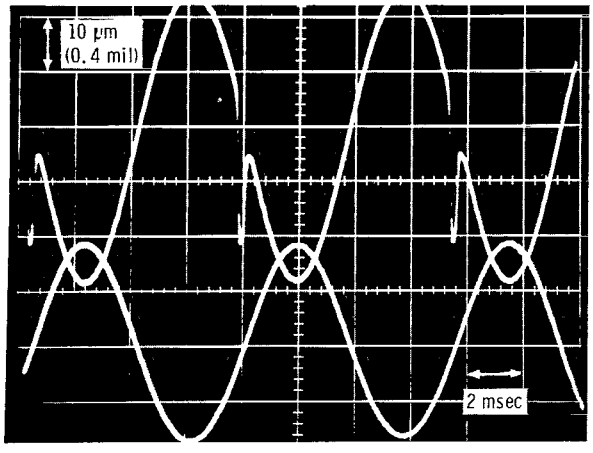

(a) Critical speed A.

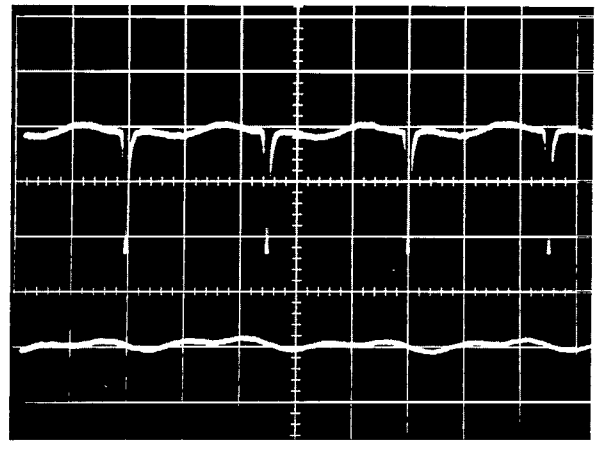

(b) Critical speed B.

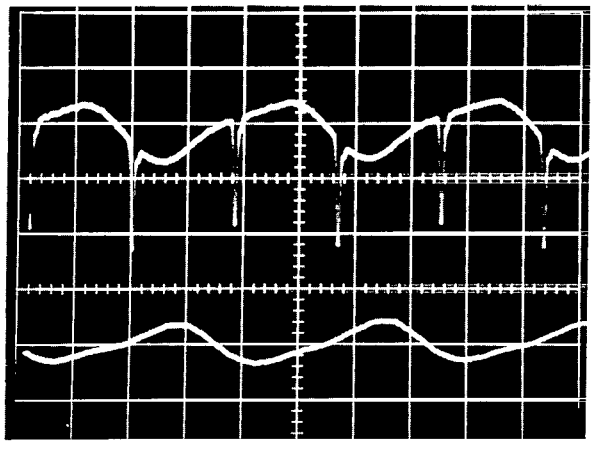

(c) Critical speed C.

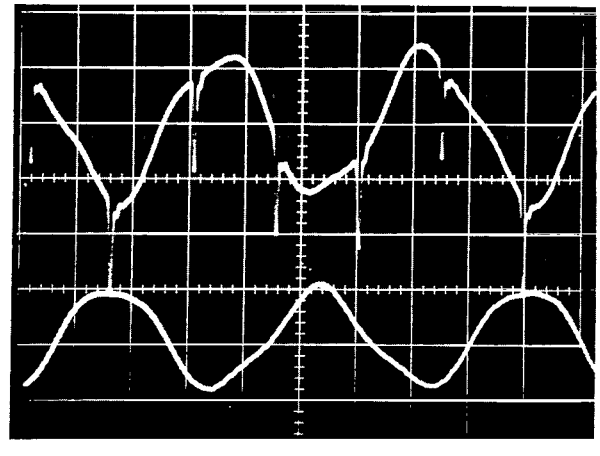

(d) Critical speed D.

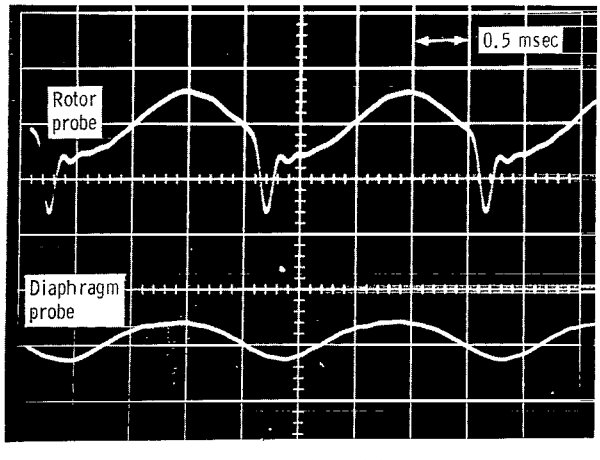

(e) Critical speed E.

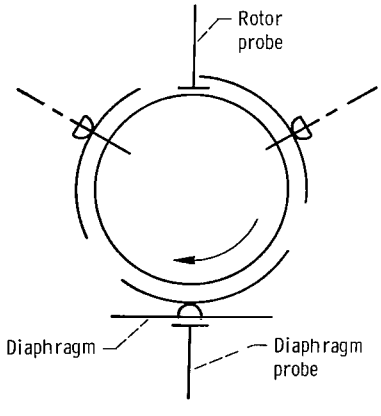

Figure 19. - Oscillographs of rotor and radial pad motion at various points in figure 7(b). Heavy mass pads with conforming pivots and pressurized operation at 410 kilonewtons per square meter (60 psig).

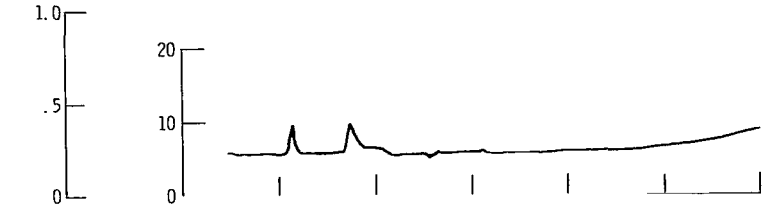

(a) Low mass pad; journal bearing supply pressure, 690 kilonewtons per square meter (100 psig).

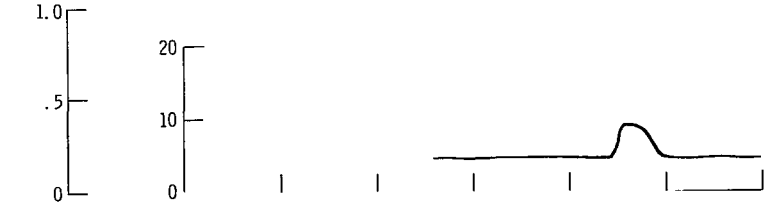

(b) Medium mass pad; journal bearing supply pressure, 280 kilonewtons per square meter (40 psig).

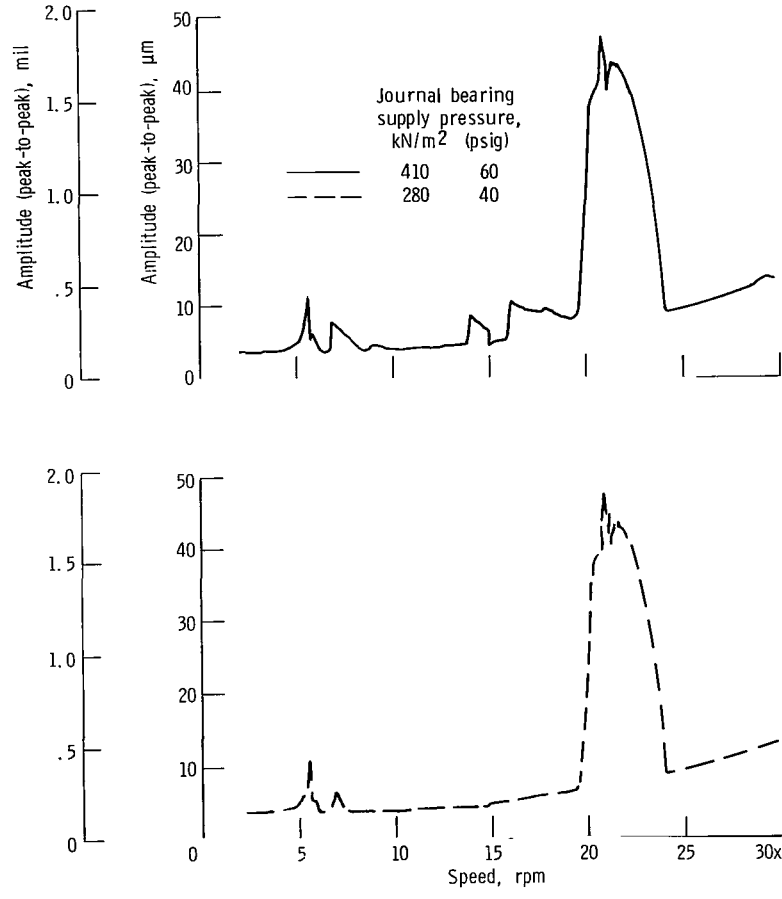

(c) Heavy mass pads.

Figure 20. - Rotor axial response with speed. Thrust bearing supply pressure, 690 kilonewtons per square meter (100 psig). ıre,

proximately 22 000 to 25 000 rpm (fig. 20(b)). With the heavy mass pads, however, a large axial vibration of the rotor occurred at about 20 000 to 23 500 rpm. This is shown in figures 20(c) and 21 where maximum amplitude of vibration reached was about 50 micrometers (2.0 mils). The rotor critical speeds, resonances, and rotor journal orbit growth affect the axial response slightly at lower speeds (figs. 20(a) and (c)).

Photographs in figure 21 show the rotor axial response with a marker on the end of the shaft that produces a small blip as it goes over the axial capacitance probe. One revolution of the rotor produces one blip on the trace. The small axial resonances are synchronous. The large axial resonance, however, was nonsynchronous, and its frequency

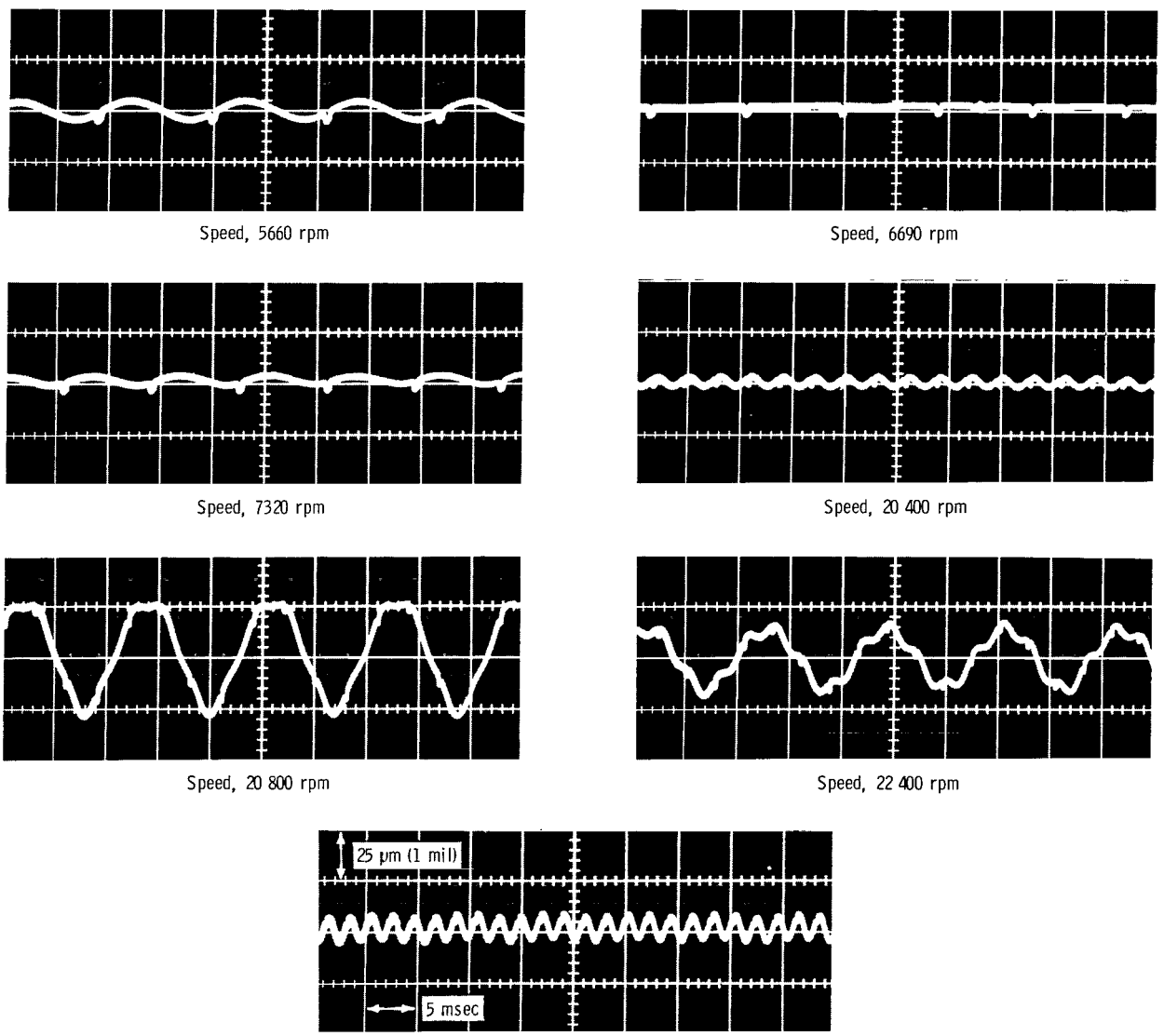

Figure 21. - Oscillographs of rotor axial response at various speeds for heavy mass pads.

was one-fourth that of the shaft speed, or about 5000 to 6000 cycles per minute.

The reason for the axial response is not evident. The thrust bearing was the same in all cases. The rotors were not always the same, but the rotor that produced a response with the heavy mass pads did not produce a response with the light mass pad.

The large axial resonance occurs in a speed range that is just above the speed range where large radial motions occur. On coastdown, the axial resonance ends abruptly at about 20 000 rpm, and the radial resonance begins abruptly at the same speed. Bending of the shaft produces a nutating surface at the thrust bearing, which could be a source of the excitation for the rotor axial resonance.

The tilting-pad journal bearing supply pressure did not seem to have any effect on the maximum amplitude of rotor axial motion. Also, a reduction in the supply pressure to the thrust bearing did not affect the axial rotor response.

Self-Acting Operation

Rotor response. - Figure 22 shows the rotor response during self-acting operation and pressurized operation with heavy mass pads and nonconforming O-ring pivots. Self-

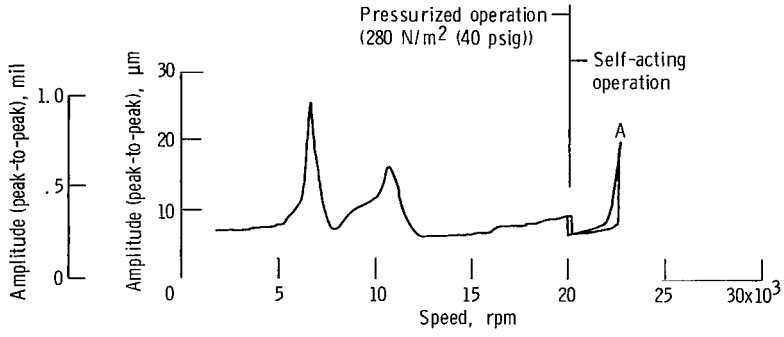

Figure 22. - Rotor response to residual unbalance under self-acting operation with heavy mass pads and nonconforming (O-ring) pivot as detected by rotor probe X.

acting operation can be attempted only above 20 000 rpm because of the heavy preload. It was surprising that a resonance started to develop with zero supply pressure after resonance was eliminated with lowering of supply pressure to 280 kilonewtons per square meter (40 psig) (fig. 15). This self-acting resonance (fig. 23) was of the type found at point D in figure 7(b) with 5 shaft revolutions per cycle of resonance.

Bearing surface rub. - Surface rub failures were experienced during self-acting operation with both rotors b and c. Neither rotor had a heat shunt inside the rotor at the

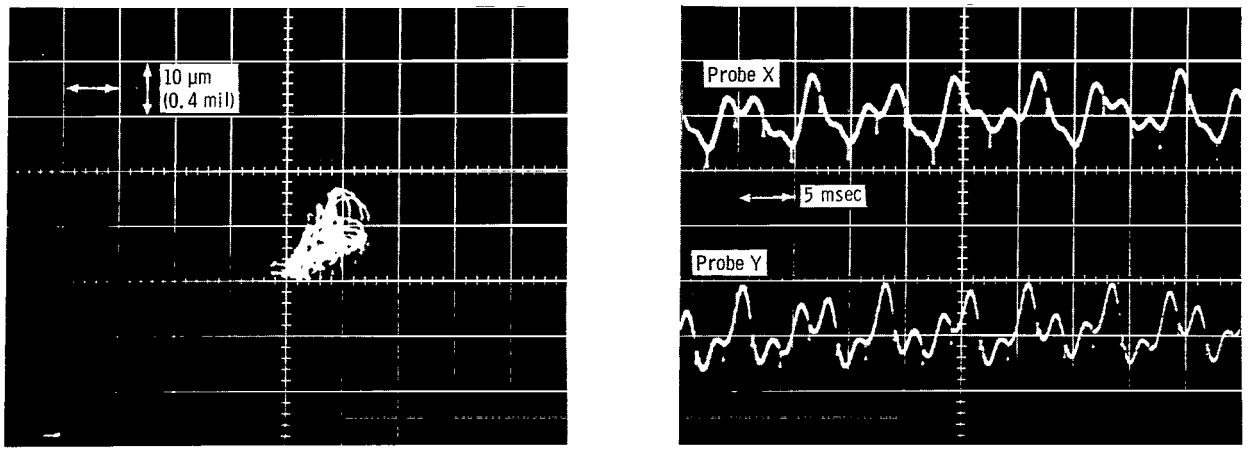

Figure 23. - Oscillographs of rotor motion at point A in figure 22.

journal locations. A typical rub failure of the pad and rotor surfaces is shown in figure 24. The pads in figure 24(b) are the heavy mass pads. The pads shown in figure 24(a) with the rotor are the light mass pads.

Shear heating of the air film in the bearing clearance space causes the hollow rotor to expand more at the centerline of the pads, which results in a crowned rotor surface. When crowning exceeds the minimum film thickness, usually at the pivot location, rubbing occurs between the rotor and the pad. Greatest damage to the rotor surface occurs in a continuous narrow band in an area at the height of the crown. On the pad surface the damage is greatest at the pivot location. Some rubbing occurred at the side edges of the pads and the corresponding areas on the rotor. Probably during rubbing at the crown, the pads are rocked in the roll mode. With rubbing, the rotor speed drops, and the pressurization system is automatically actuated. The turbine drive is shut off, and the rotor coasts down in speed.

Rubbing did not cause excessive surface damage, and pressurized operation was possible during coastdown and later. The rotor response during and after damage is shown in the photographs in figure 25. It shows that amplitudes are larger for both radial and axial rotor motions because of the rubbing.

High Speed Rotor Bending

To determine the cause of the shaft orbit growth starting about 15 000 rpm, two capacitance probes were added to the existing two probes, which observed the rotor motion.

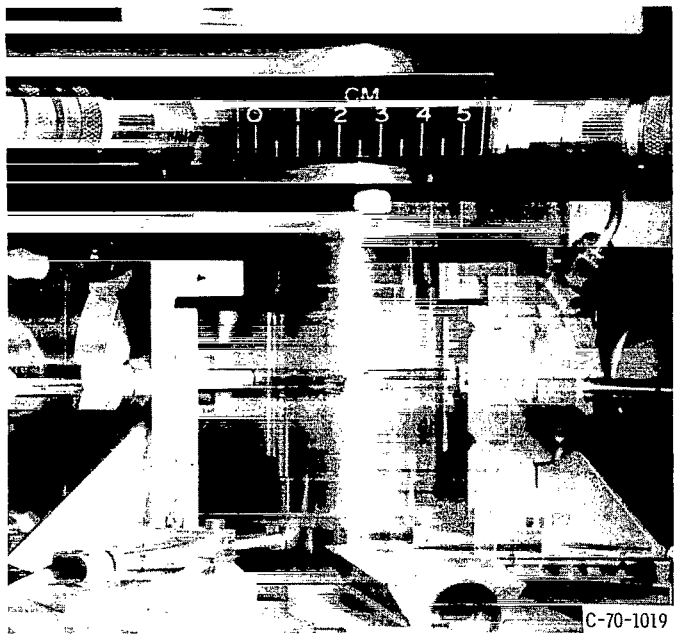

(a) Rotor.

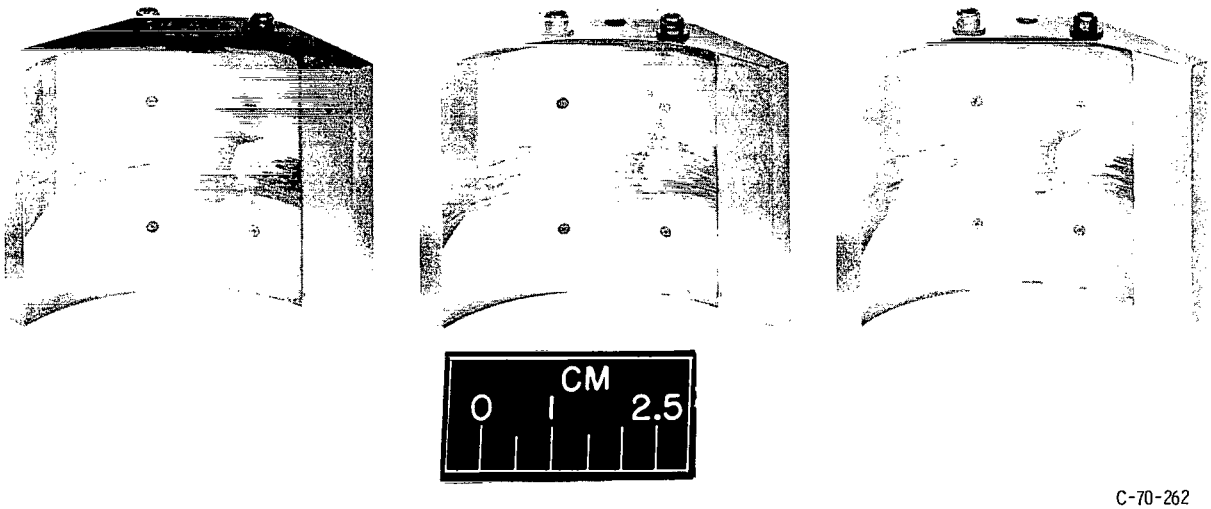

Fixed mounted pad 1

Flexure (diaphragm) mounted pad 2

Fixed mounted pad 3

(b) Bearing pads.

Figure 24. - Typical bearing rub failure.

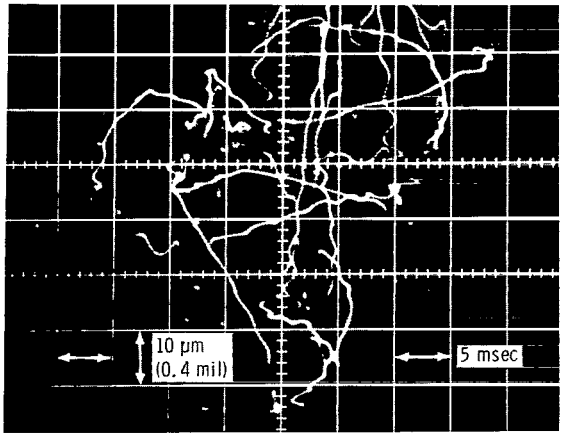

(a) Rotor orbit at rub; self-acting operation of the journal bearing.

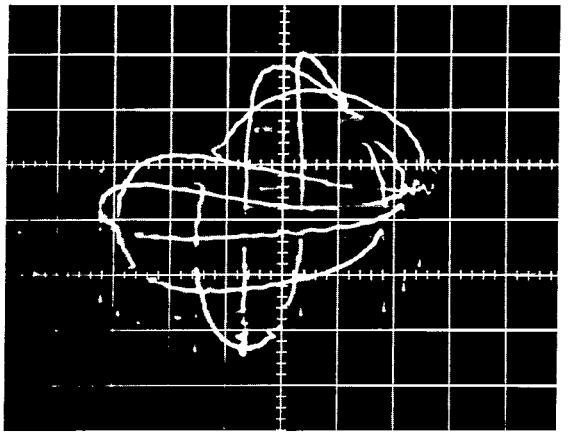

(b) Rotor orbit at 16 600 rpm after rub on coastdown; journal bearing supply pressure, 410 kilonewtons per square meter.

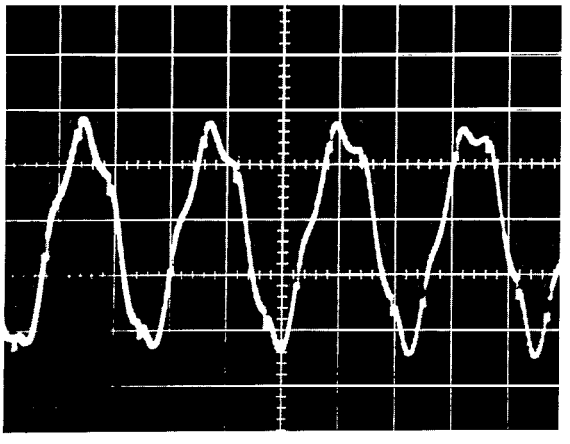

(c) Rotor axial response at 21 500 rpm after rub on coastdown; journal bearing supply pressure, 410 kilonewtons per square meter.

Figure 25. - Rotor response at pad and coastdown after rub. Heavy mass pads and conforming pivot. Thrust bearing supply pressure, 690 kilonewtons per square meter (100 psig).

All four probes were in line. Rotor probes 2 and 4 were located at the side of the bearing. The data obtained with four probes shown in figure 26 and in the photographs of figure 27 indicated that the rotor was bending and that the bending increased with increasing speed. Coincidentally, the nodal points in bending occurred almost at the bearing centerlines (fig. 26) so that the bearing pads were not subjected to as much rotor motion as was indicated by the capacitance probe data.

Figure 28 illustrates the possible result when material is removed in line at the ends of the shaft to obtain rigid-body balance. At high speeds the centrifugal loading can cause shaft bending. To prevent high-speed rotor bending, balancing should be accomplished by removing material in the plane of unbalance. A more rigid, shorter shaft can also reduce high speed bending.

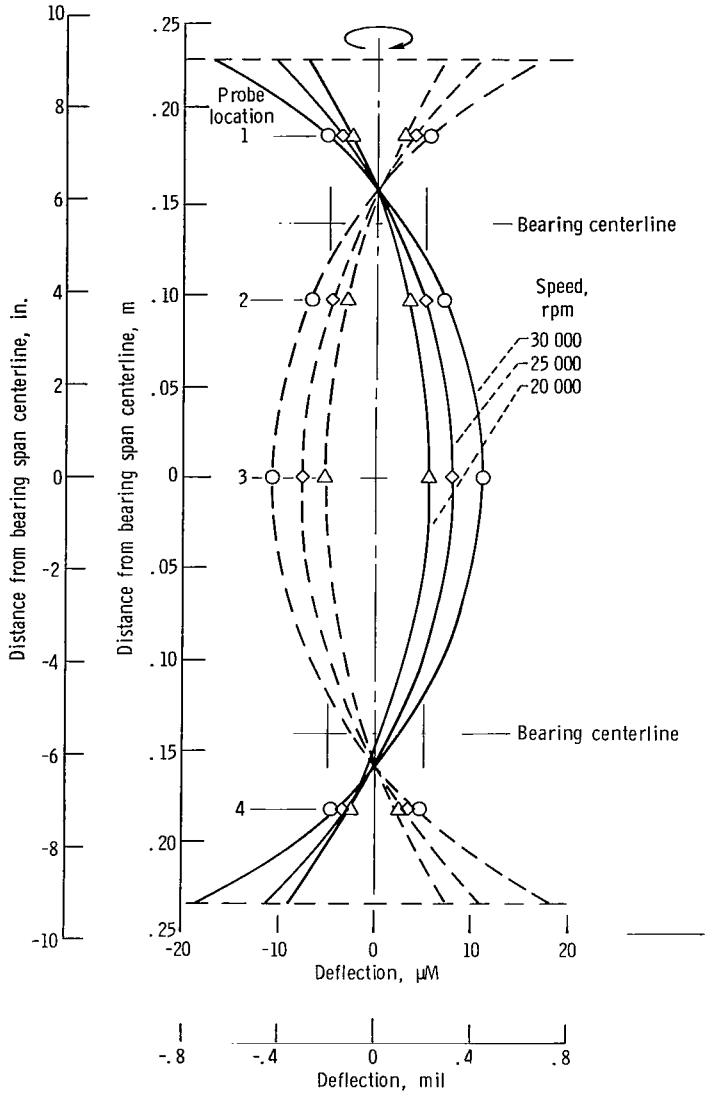

Figure 26. - Shaft bend with rotation.

Two of the three rotors used in this investigation exhibited bending at high speeds. These two rotors were used in conjunction with the low and heavy mass pads. The excitations seen by the low and heavy mass pads were therefore similar, so that a direct comparison of their high-speed dynamic behavior is valid. Additionally, the effect of rotor bending on pad behavior is considered to be of secondary importance because the bearings were located very close to the nodal points.

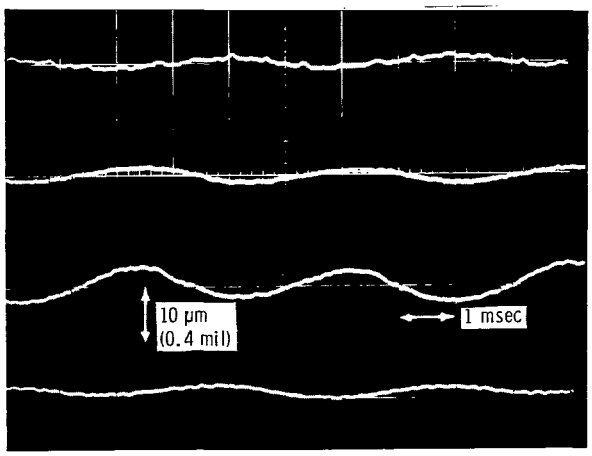

Speed, 15 000 rpm

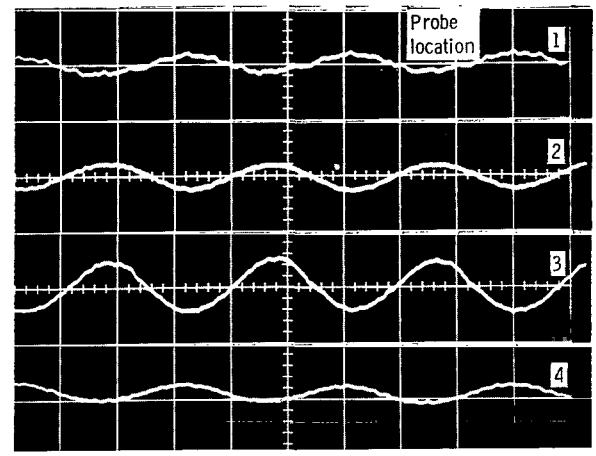

Speed, 20 000 rpm

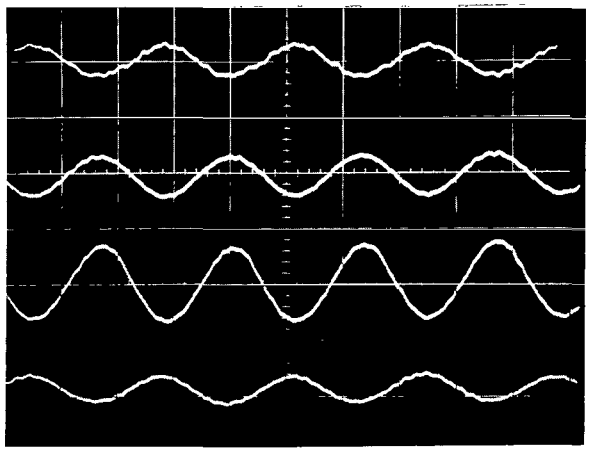

Speed, 25 000 rpm

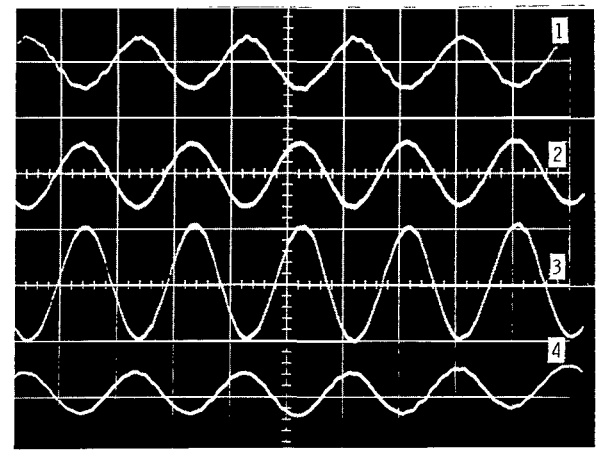

Speed, 30 000 rpm

Figure 27. - Shaft deflection at four speeds at various probe locations along the length of the shaft.

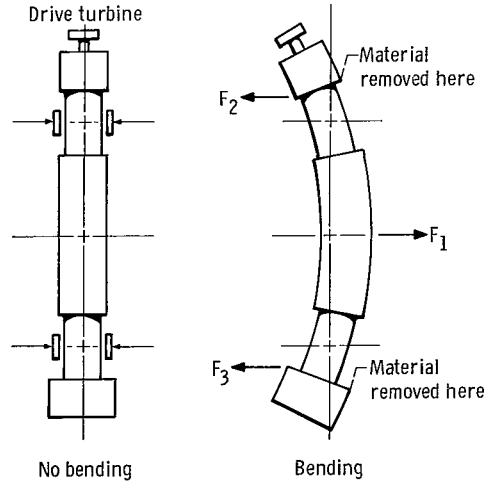

Figure 28. - Sketch illustrating high-speed rotor bending.

SUMMARY OF RESULTS

A series of rotor-bearing dynamic tests was run with vertically oriented rotors supported with two three-pad tilting-pad gas journal bearings and a simple pressurized thrust bearing. The journal pads contained orifices for pressurized operation and were operated in both the pressurized and self-acting modes. The bearing pads were 5.1 centimeters (2.02 in.) in diameter and 3.8 centimeters (1.50 in.) long. The length to diameter ratio was 0.75. Each pad was individually pivoted with one pivot in each bearing flexure mounted and two pivots rigidly mounted. Three pad masses and two pivot geometries were compared. Rotors with and without internal heat shunts at the journal bearing locations were used. Tests were conducted with air as the lubricant over a range of external supply pressures from 0 to 690 kilonewtons per square meter (100 psig) and a speed range of 0 to 38 500 rpm. The flexure stiffness was approximately 760 kilonewtons per meter (4300 lbf/in.). The tilting-pad bearings were set up with a zero speed clamping load of 53 newtons (12 lbf). The following results were obtained:

1. The heavy mass pad assembly (pad plus pivot) produced three rotor-bearing resonances above the first two rotor critical speeds. The resonances occurred at approximately two, two and one half, and four times the first critical speed.

2. The frequency of the first resonance was one half, the second resonance one fifth, and the third resonance one fourth of the shaft rotational frequency. The three resonance orbit speeds were nonsynchronous.

3. The orientation of the orbits at resonance was primarily in the direction of the diaphragm flexure (perpendicular to the face of the flexure). At the second resonance, the orbit was a combination of rotor motion perpendicular and parallel to the face of the diaphragm flexure.

4. The resonances due to high mass pad were eliminated by reduced supply pressure.

5. Rotor resonances above the shaft first two critical speeds did not occur with the low mass pad assembly.

6. Bearing pad response was to track the motion of the rotor for all pads investigated at all speeds.

7. The effect of pivot geometry (conforming and nonconforming) was primarily one of weight addition to the total mass of the pad pivot assembly.

8. Pivot surface damage was minimal for the two geometry pivots except for the nonconforming pivot under the conditions of high supply pressure and operation through the first critical speed. Impact damage occurred to the rigidly mounted pivots but not to the flexure mounted pivot.

9. Self-acting operation of the tilting-pad journal bearings with rotors that did not have internal heat shunts resulted in rub failure between the bearing surfaces at the center of the bearing width.

10. Shaft bending occurred in two of the three rotors that were balanced as a rigid body at low speeds in planes other than the unbalance planes. Shaft bending produced large orbits at the bearing locations, and this limited the speed of operation.

11. Large axial rotor resonance was present at one fourth the shaft speed for the heavy mass pad journal bearings in the speed range of 20 000 to 23 500 rpm (above the large radial resonances).

Lewis Research Center,
National Aeronautics and Space Administration,
Cleveland, Ohio, September 22, 1971,
114-03.

REFERENCES

1. Anon.: Design and Fabrication of a High-Performance Brayton Cycle Radial-Flow Gas Generator. NASA CR-706, 1967.
2. Anon.: Design and Fabrication of the Brayton Rotating Unit (BRU). Rep. APS-5334-R, AiResearch Mfg. Co., Mar. 15, 1971.
3. Sternlicht, Beno; and Arwas, Elie B.: Modern Gas-Bearings Turbomachinery. Part 1: The State-of-the-Art. Mech. Eng., vol. 88, no. 1, Jan. 1966, pp. 24-29.
4. Sternlicht, Beno; and Arwas, Elie B.: Modern Gas-Bearings Turbomachinery. Part 2: Research and Application. Mech. Eng., vol. 88, no. 2, Feb. 1966, pp. 42-48.
5. Curwen, P. W.; Jones, H. F.; and Schwarz, H.: Application of Gas Bearings to Closed-System Brayton-Cycle Turbomachinery - Recent Accomplishments and Potential Problem Areas. J. Eng. Power, vol. 88, no. 4, Oct. 1966, pp. 367-377.
6. Gunter, E. J., Jr.; Hinkle, J. G.; and Fuller, D. D.: The Effects of Speed, Load, and Film Thickness on the Performance of Gas-Lubricated, Tilting-Pad Journal Bearings. ASLE Trans., vol. 7, no. 4, Oct. 1964, pp. 353-365.

7. Nemeth, Zolton N.; and Anderson, W. J.: Dynamic Behavior of Air Lubricated Pivoted-Pad Journal Bearing-Rotor System. I - Effects of Mount Stiffness and Damping. NASA TN D-5685, 1970.

8. Wong, R. Y.; Stewart, W. L.; and Rohlik, H. E.: Pivoted-Pad Journal Gas Bearing Performance in Exploratory Operation of Brayton Cycle Turbocompressor. J. Lubr. Tech., vol. 90, no. 4, Oct. 1968, pp. 687-696.

9. Anon.: Basic Applied Research in Fluid Power Control. Massachusetts Inst. Tech. (RTD-TDR-63-4252, DDC AD-435774), Feb. 1964.

10. Chu, T. Y.; McCabe, J. T.; and Elrod, H. G.: Stability Considerations for a Gas-Lubricated Tilting-Pad Journal Bearing. Part I: Analytical Methods. J. Lubr. Tech., vol. 90, no. 1, Jan. 1968, pp. 162-172.

NASA-Langley, 1972 — 15 E-6336

"The aeronautical and space activities of the United States shall be conducted so as to contribute . . . to the expansion of human knowledge of phenomena in the atmosphere and space. The Administration shall provide for the widest practicable and appropriate dissemination of information concerning its activities and the results thereof."

—NATIONAL AERONAUTICS AND SPACE ACT OF 1958

NASA SCIENTIFIC AND TECHNICAL PUBLICATIONS

TECHNICAL REPORTS: Scientific and technical information considered important, complete, and a lasting contribution to existing knowledge.

TECHNICAL NOTES: Information less broad in scope but nevertheless of importance as a contribution to existing knowledge.

TECHNICAL MEMORANDUMS: Information receiving limited distribution because of preliminary data, security classification, or other reasons.

CONTRACTOR REPORTS: Scientific and technical information generated under a NASA contract or grant and considered an important contribution to existing knowledge.

TECHNICAL TRANSLATIONS: Information published in a foreign language considered to merit NASA distribution in English.

SPECIAL PUBLICATIONS: Information derived from or of value to NASA activities. Publications include conference proceedings, monographs, data compilations, handbooks, sourcebooks, and special bibliographies.

TECHNOLOGY UTILIZATION PUBLICATIONS: Information on technology used by NASA that may be of particular interest in commercial and other non-aerospace applications. Publications include Tech Briefs, Technology Utilization Reports and Technology Surveys.

Details on the availability of these publications may be obtained from:

SCIENTIFIC AND TECHNICAL INFORMATION OFFICE

NATIONAL AERONAUTICS AND SPACE ADMINISTRATION

Washington, D.C. 20546